SELF-ASSEMBLY STUDIES AND STABILITY EVALUATION OF BRANCHED-CHAIN GLYCOLIPID NANOPARTICLES

SYAIDATUL ATIQAH BINTI SAZALEE

FACULTY OF SCIENCE
UNIVERSITY OF MALAYA
KUALA LUMPUR

2019

SELF-ASSEMBLY STUDIES AND STABILITY EVALUATION OF BRANCHED-CHAIN GLYCOLIPID NANOPARTICLES

SYAIDATUL ATIQAH BINTI SAZALEE

DISSERTATION SUBMITTED IN FULFILMENT OF THE REQUIREMENTS FOR THE DEGREE OF MASTER OF SCIENCE

DEPARTMENT OF CHEMISTRY
FACULTY OF SCIENCE
UNIVERSITY OF MALAYA
KUALA LUMPUR

2019

UNIVERSITY OF MALAYA
ORIGINAL LITERARY WORK DECLARATION

Name of Candidate: **SYAIDATUL ATIQAH BINTI SAZALEE**

Matric No: **SGR140080**

Name of Degree: **MASTER OF SCIENCE**

Title of Project Paper/Research Report/Dissertation/Thesis ("this Work"):

SELF-ASSEMBLY STUDIES AND STABILITY EVALUATION OF BRANCHED-CHAIN GLYCOLIPID NANOPARTICLES

Field of Study: **PHYSICAL CHEMISTRY**

I do solemnly and sincerely declare that:

(1) I am the sole author/writer of this Work;
(2) This Work is original;
(3) Any use of any work in which copyright exists was done by way of fair dealing and for permitted purposes and any excerpt or extract from, or reference to or reproduction of any copyright work has been disclosed expressly and sufficiently and the title of the Work and its authorship have been acknowledged in this Work;
(4) I do not have any actual knowledge nor do I ought reasonably to know that the making of this work constitutes an infringement of any copyright work;
(5) I hereby assign all and every rights in the copyright to this Work to the University of Malaya ("UM"), who henceforth shall be owner of the copyright in this Work and that any reproduction or use in any form or by any means whatsoever is prohibited without the written consent of UM having been first had and obtained;
(6) I am fully aware that if in the course of making this Work I have infringed any copyright whether intentionally or otherwise, I may be subject to legal action or any other action as may be determined by UM.

Candidate's Signature   Date:

Subscribed and solemnly declared before,

Witness's Signature   Date:

Name:

Designation:

SELF-ASSEMBLY STUDIES AND STABILITY EVALUATION OF BRANCHED-CHAIN GLYCOLIPID NANOPARTICLES

ABSTRACT

Sugar-based surfactants are more prominent due to their nonionic and bio-based properties. Glycolipids such as alkyl polyglucosides (APGs) are amongst the most popular because they can be found in nature or synthesised from cheap natural resources. This research investigates the liquid crystalline and self-assembly properties of a branched-chain glycolipid namely 2-hexyldecyl-$\beta(/\alpha)$-D-glucoside ($\alpha\beta$-Glu-OC$_{10}$C$_6$). The thermotropic and lyotropic liquid crystalline phases were determined using differential scanning calorimetry (DSC), optical polarising microscope (OPM) and small-angle X-ray scattering (SAXS). In dry conditions, $\alpha\beta$-Glu-OC$_{10}$C$_6$ formed a columnar phase with a focal conic texture, while in a binary aqueous system, $\alpha\beta$-Glu-OC$_{10}$C$_6$ formed inverse hexagonal dispersion called hexosome. The critical aggregation concentrations (CACs) for the branched-chain glycolipid and when it mixed with nonionic co-surfactants (Tween series: T20, T40, T60 and T80) were investigated by using surface tensiometer. The addition of co-surfactants to the glycolipid dispersions reduced the CAC value of $\alpha\beta$-Glu-OC$_{10}$C$_6$, which further stabilised the system. The formation of mixed surfactants hexosomes was further investigated in terms of the particle size and morphology by using a particle sizer and a transmission electron microscope (TEM). By using light backscattering measurements for 24 h, the stability of the hexosomes was analysed to determine the destabilisation of the system *vis-à-vis* particle size variations and particle migration. Furthermore, hexosomes based on the hydrophobic surfactant; $\alpha\beta$-Glu-OC$_{10}$C$_6$, could be insufficiently stabilised, due to the fact that hydrophilic-lipophilic balance (HLB) of the surfactant preventing the formation of a stable double layer, as previously reported. The stability of $\alpha\beta$-Glu-OC$_{10}$C$_6$ hexosomes were enhanced via the

addition of co-surfactant Tween series, which also subsequently decrease particle sizes, thus increasing stability. Therefore, T80 is the most stable co-surfactant to the $\alpha\beta$-Glu-OC$_{10}$C$_6$ hexosomes formation compared to other co-surfactant. The findings suggest the branched-chain glycolipid as a possible alternative to nonionic surfactant for drug carrier system applications in the near future.

Keywords: Branched-chain glycolipid, nonionic surfactant, inverse hexagonal phase, hexosome, stability

KAJIAN PERHIMPUNAN DIRI DAN PENILAIAN KESTABILAN

NANOPARTIKEL GLIKOLIPID RANTAIAN BERCABANG

ABSTRAK

Surfaktan berasaskan gula kini menarik perhatian kerana sifat bukan-ionik dan biologinya. Glikolipid seperti alkil poliglukosida (APG) adalah paling popular kerana ia boleh didapati dalam alam semulajadi atau disintesis dari sumber semulajadi yang murah. Penyelidikan ini mengkaji ciri-ciri kristal cecair dan perhimpunan diri glikolipid rantaian bercabang iaitu 2-heksildesil-$\beta(/\alpha)$-D-glukosida ($\alpha\beta$-Glu-OC$_{10}$C$_6$). Fasa kristal cecair termotropik dan liotropik dikaji dengan menggunakan imbasan pembezaan kalorimeter (DSC), mikroskop optik berpolar (OPM) dan serakan X-ray bersudut kecil (SAXS). Dalam keadaan kering, $\alpha\beta$-Glu-OC$_{10}$C$_6$ memberi fasa kolumnar bertekstur fokal konik, manakala dalam sistem binari akueus, $\alpha\beta$-Glu-OC$_{10}$C$_6$ membentuk penyebaran heksagon terbalik yang dikenali sebagai heksosom. Kepekatan agregasi kritikal (CACs) bagi glikolipid rantaian bercabang dan apabila ianya bercampur dengan surfaktan bersama bukan-ionik (siri Tween: T20, T40, T60 dan T80) telah dikaji menggunakan pengukur tegangan permukaan. Penambahan surfaktan bersama kepada penyebaran glikolipid ini telah mengurang nilai kepekatan agregasi kritikal (CAC) $\alpha\beta$-Glu-OC$_{10}$C$_6$, dimana mengakibatkan sistem menjadi lebih stabil. Pembentukan heksosom hasil dari campuran surfaktan telah dikaji dengan lebih lanjut dari segi saiz zarah dan morfologinya dengan menggunakan pengukur zarah dan mikroskop penyebaran elektron (TEM). Dengan menggunakan pengukuran serakan cahaya berbalik (light backscattering) selama 24 jam, kestabilan heksosom telah dikaji selanjutnya bagi mengesan ketidakstabilan sistem dengan menghubungkannya dengan variasi saiz zarah dan penghijrahan zarah. Selanjutnya, heksosom yang terhasil dari surfaktan hidrofobik; $\alpha\beta$-Glu-OC$_{10}$C$_6$ mungkin tidak cukup stabil, kerana keseimbangan hidrofilik-lipofiliknya (HLB) surfaktan tidak

membetuk lapisan berganda yang stabil seperti dilaporkan sebelum ini. Kestabilan heksosom $\alpha\beta$-Glu-OC$_{10}$C$_6$ dipertingkat dengan menambah siri surfaktan bersama Tween yang seterusnya mengurangkan saiz zarah dengan itu meningkatkan kestabilannya. Oleh itu, T80 adalah surfaktan bersama yang paling stabil kepada pembentukan heksosom $\alpha\beta$-Glu-OC$_{10}$C$_6$ berbanding dengan surfaktan bersama yang lain. Penemuan ini mencadangkan bahawa glikolipid rantaian bercabang sebagai alternatif yang mungkin bagi surfaktan bukan-ionik untuk aplikasi sistem pembawa ubat pada masa terdekat.

Kata kunci: Glikolipid rantai bercabang, surfaktan bukan-ionic, heksagon terbalik, heksosom, kestabilan

ACKNOWLEDGEMENTS

TABLE OF CONTENTS

LIST OF FIGURES

LIST OF TABLES

LIST OF EQUATIONS

LIST OF SYMBOLS AND ABBREVIATIONS

% (w/w)	:	Mass fraction
α	:	Alpha
β	:	Beta
BS	:	Backscattered
ca.	:	Approximately
CAC	:	Critical Aggregation Concentration
CMC	:	Critical Micellar Concentration
CPP	:	Critical packing parameter
Cr	:	Crystalline phase
DLS	:	Dynamic Light Scattering
DMSO	:	Dimethyl sulfoxide
DSC	:	Differential Scanning Calorimeter
e.g	:	Exempli gratia; for example
etc	:	Et cetera; and the others
FTIR	:	Fourier Transform Infrared Spectroscopy
GMO	:	Glycerol monooleate
GTO	:	Glycerol trioleate
h	:	Hour
ΔH	:	Enthalpy
H_I	:	Normal hexagonal phase
H_{II}	:	Inverse hexagonal phase
HLB	:	Hydrophilic-lipophilic balance
L	:	Isotropic phase
$L\alpha$	:	Lamellar liquid crystal phase

LLC	:	Lyotropic liquid crystal
N	:	Nematic phase
N*	:	Cholesteric
NA	:	Not available
NMR	:	Nuclear Magnetic Resonance
OG	:	Oleyl glycerate
OPM	:	Optical Polarising Microscope
Phyt	:	Phytantriol
PDI	:	Polydispersity index
PEG	:	Polyethylene glycol
PG	:	Phytanyl glycerate
r.d	:	Radiation damaged
S	:	Order parameter
SmA	:	Smectic A phase
SmC	:	Smectic C phase
SAXS	:	Small Angle X-ray Scattering
T20	:	Tween 20
T40	:	Tween 40
T60	:	Tween 60
T80	:	Tween 80
TAG	:	Tricaprylin
TGA	:	Thermogravimetric Analyser
TEM	:	Transmission Electron Microscope

LIST OF APPENDIX

CHAPTER 1: INTRODUCTION

1.1 General Introduction

Modern future medicine will enable people to live longer and healthier with the use of personalised or tailor design drugs (Castaldo & Capasso, 2002; Crommelin et al., 2011; Murthy, 2007). This future medicine is afforded by the development of better drug and improved delivery nanotechnology where choosing the efficient biosurfactant is an important step. Examples of these biosurfactants are glycolipids which have been extensively studied because their production yields are much higher than other biosurfactants (Kitamoto et al., 2002a; Kitamoto et al., 2009b). Glycolipids may be obtained from both natural products and synthetic process, but synthetic glycolipids are highly in demand due to interest in biomimicking research (Ahmad et al., 2012; Revathi & Dhanaraju, 2014) especially in the development of cosmetic and pharmaceutics exploiting special features of the materials including their liquid crystal phases (Hirlekar et al., 2010; Kulkarni, 2016). Thus in this chapter, we begin by introducing glycolipids and their associations to the many possible exotic liquid crystals phases.

1.2 Surfactant

The word "surfactant" is an abbreviation for surface active agent, which means an employed in technical system in order to overcome solubility problem, as dispersants, as emulsifiers or to modify surfaces (Holmberg, 2001). Surfactants are amphiphile which a word derived from the Greek word "amphi" meaning both and all surfactant molecules consist of lyophilic part which is soluble in a specific fluid and other is lyophobic part (Kronberg & Lindman, 2003). In contrast, when fluid is water it does consist of hydrophilic headgroup (water liking) and hydrophobic tail (water hating) as shown in **Figure 1.1**. Last decades, the extension of surfactant application to such high-technology

area widely used such as viral research, electronic printing, biotechnology, magnetic recording and micro-electronic (Rosen & Kunjappu, 2004). Besides, surfactant also can be used in daily life such as pharmaceutical products, motor oils (automobiles), petroleum, detergents and flotation agents (ores). Thus, surfactants are found to be versatile products and have a various ranges of applications for necessity and human needs.

Hydrophilic part

Hydrophobic part
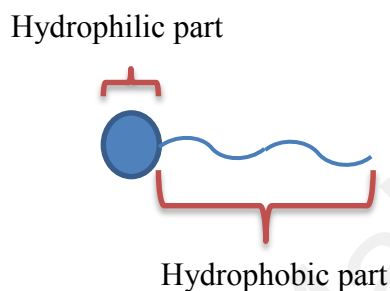
Figure 1.1: An illustration of an amphiphilic surfactant.

In general, surfactants are classified based on the nature of the headgroup as its carries a net charge. If the charge is negative, it is called anionic while if the charge is positive, the surfactant called cationic. However, if charge contains both oppositely it is called zwitterionic and nonionic surfactant has no charge group. In solution, they self-assemble to form a various structures from the order of nano to micro ranges (Sagar et al., 2007). Nonionic surfactants are the most common type of surface active agent used in preparing vesicles due to advantages stability, toxicity and compatibility than other type of surfactants (Kumar & Rajeshwarrao, 2011). They are generally less toxic, less haemolytic and less aggravating to cellular surfaces and prone to maintain near physiological pH in solution. Moreover, nonionic surfactants are consisting of both polar and non-polar segment and have higher interfacial activity. The following are brief descriptions of the classes of surfactant:

Anionic Surfactant

Anionic surfactant is dissociated in water for an amphiphilic anion and a cation which is in general an alkaline metal (Na^+, K^+) or a quaternary ammonium. It contains functional groups at surfactant headgroup, such as sulfonate, phosphate, sulphate and carboxylates (Salager, 2002). Some commonly agent include alkyl benzene sulfonates (detergents), lauryl sulphate (foaming agent), fatty acid (soap), di-alkyl sulfosuccinate (wetting agent), lignosulfonates (dispersant) etc. The commercial anionic surfactants are sodium dodecyl sulphate (SDS), also known as sodium lauryl ether sulphate (SLES) and sodium bis (2-ethyl hexyl) sulfosuccinate (AOT) as shown in **Figure 1.2** (Farn, 2008; Kronberg & Lindman, 2003; Salager, 2002).

Sodium dodecyl sulphate (SDS)

Sodium bis (2-ethyl hexyl) sulfosuccinate (AOT)
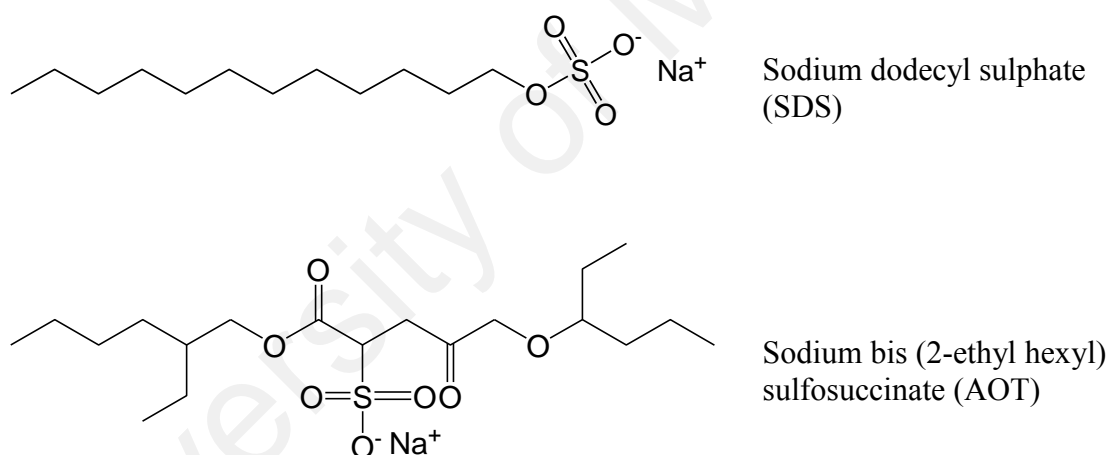
Figure 1.2: Commercial anionic surfactants.

Cationic Surfactant

Cationic surfactant are comprised of a positively charged headgroup and dissociated in water into amphiphilic cation and an anion, often of halogen type (Farn, 2008; Kronberg & Lindman, 2003). Most of cationic surfactants applied as anti-microbials and anti-fungals. This classes corresponds to nitrogen compounds such as fatty acid and quaternary ammonium cations includes cetylpyridinium chloride and cetyl trimethylammonium bromide (CTAB) (**Figure 1.3**) (Rosen & Kunjappu, 2004; Salager, 2002).

Cetylpyridinium chloride   Cetyl trimethylammonium bromide (CTAB)
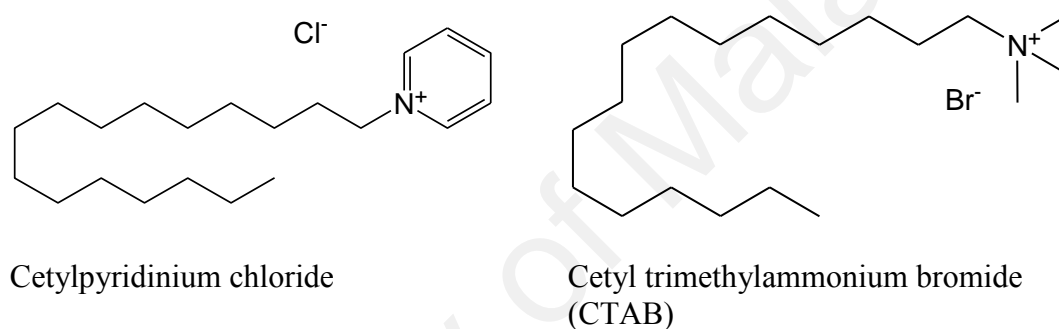
Figure 1.3: Examples of cationic surfactants.

Zwitterionic Surfactant

When surfactant exhibits both cationic (positive) and anionic (negative) centers attached to the same molecule it is called zwitterionic or amphoteric (Salager, 2002). The anionic part can be variable and include sulfonates. The cationic part is based on primary, secondary, or tertiary amines or quaternary ammonium cations. Zwitterionic surfactants are often sensitive to pH and will behave as anionic or cationic based on pH (Farn, 2008; Rosen & Kunjappu, 2004). Cocamidopropyl betaine has a carboxylate with the ammonium is an example of zwitterionic surfactant as depicted in **Figure 1.4** (Salager, 2002).
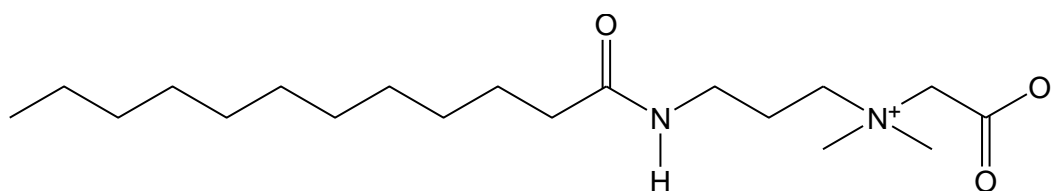
Cocamidopropyl betaine

Figure 1.4: Example of zwitterionic surfactant.

Nonionic Surfactant

Nonionic surfactant has no charge groups in its headgroup. Therefore, it do not ionise in aqueous solution because their hydrophilic group is a non-dissociate type such as phenol, ester, ether, amide or alcohol. In the past, glucoside sugar based headgroups have been introduced in the market because of their low toxicity (Kumar & Rajeshwarrao, 2011; Salager, 2002). As for lipophilic group, it is often of the alkyl or alkylbenzene type, the former coming from fatty acids of natural origin. The commercial of nonionic surfactants are Span 20 and Brij 35 as shown in **Figure 1.5**.
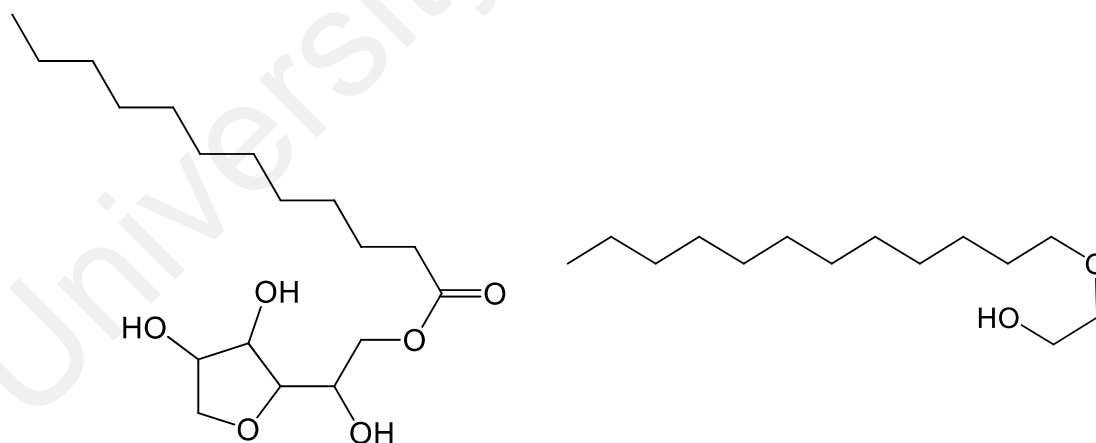
Span 20   Brij 35

Figure 1.5: Commercial nonionic surfactants.

1.3   Glycolipids

A glycoconjugate is a substance when a carbohydrate combines with a biomolecule, other than carbohydrate, for examples glycoprotein, glycopeptide, peptidoglycan and glycolipid (Allen & Kisailus, 1992; Curatolo, 1987). Glycolipid is a nonionic surfactant that can be found naturally and can be further divided into several different types such as glycoglycerolipid and glycosyl phosphopolyprenol. Moreover, glycosphingolipid which is the combination of carbohydrates with sphingoid is further subclassified into cerebroside, globoside and ganglioside. These can either have two aliphatic chains (saturated and unsaturated) attached to a sugar head group, thereby allowing molecular structures to be formed that have similar shapes to those of phospholipids (Goodby, 1998). The general chemical structures of these glycosphingolipids are shown in **Figure 1.6**.

GAL (1 ➤ 3) GALNac (1 ➤ 4) GLU (1 ➤ 1) Ceramic Unit

GAL = Galactose
GALNac = N-acetyl galactominase   a/Ganglioside
GLU = Glucose
Ceramide = N-acyl sphingosine
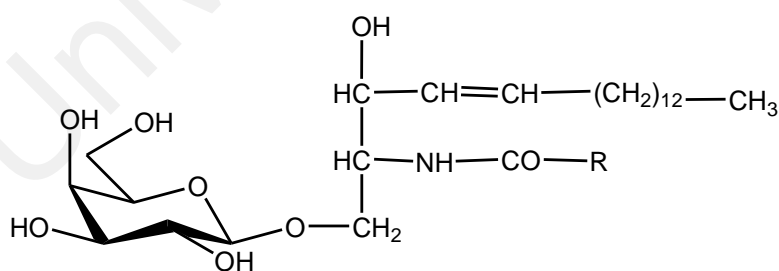
b/Galactocerebroside
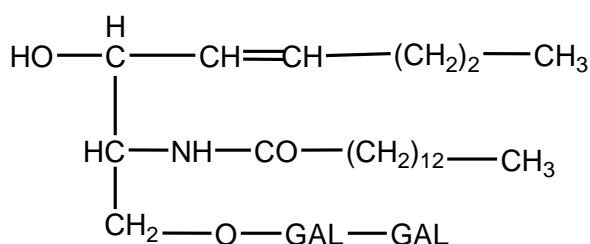
c/Globoside

Figure 1.6: Chemical structure of glycoshingolipids.

Another important class of natural glycolipids is glycoglycerolipids which are formed by the combination of carbohydrates with 1,2-di-*O*-acyl glycerols. Two glycoglycerolipids are found in the higher plant chloroplast, monogalactosyl diacylglycerol (MGDG) and digalactosyl diacylglycerol (DGDG). Another type of glycolipid is glycosyl phosphopolyprenol which is biochemically different from the other glycolipids. In this compound the phosphate bridge is unique among sugar lipid (Shibaev & Danilov, 1992). The general chemical formula of polyprenoid alcohols is shown in **Figure 1.7**.

(n varies between 5 to 24)
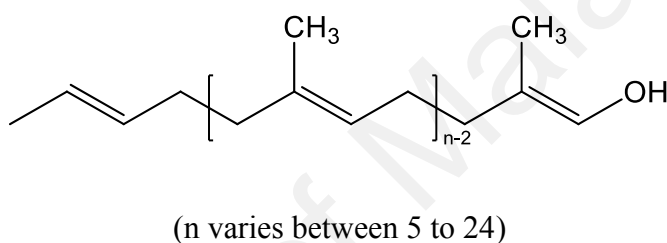
Figure 1.7: General chemical formula of polyprenoid alcohols.

1.4   Liquid Crystal

Liquid crystal is a phase intermediate between the liquid and the solid state (Dierking, 2003). Molecules in the solid state usually have both the positional and the orientational orders. When molecules possess both the positional and the orientational orders, they occupy specific lattice sites (position) and their molecular axes are in specific preferred directions (orientation). On the other hand, in liquid phase the molecules do not possess both the positional and the orientational orders. This means the molecules center of mass is randomly distributed and there is not preferred direction. In between these two states of matters (solid and liquid), liquid crystals phase possess some of the crystalline order and this is observed by comparing the latent heat value of crystal to liquid crystal transition and liquid crystal to liquid phase. Furthermore, the molecular axes in liquid crystal phase tend to point along a preferred direction, which is called director and

denoted by the vector n̂ unit (**Figure 1.8**). Order parameter, S is another parameter which describes to what degree the long axes of the molecules are aligned with the director on average and the equation is given in **Equation 1.1** (Collings & Hird, 1997).

$$S = \left< \frac{3\ cos^2\theta - 1}{2} \right> \tag{1.1}$$

where S is the order parameter and the average of $cos^2\theta$ where θ is the angle between the director and long axes of liquid crystal molecules or mesogens and the relationship between order parameter and director is shown in **Figure 1.8**.
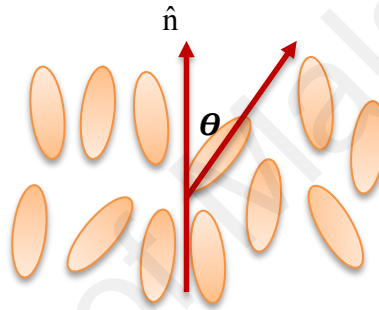
Figure 1.8: A schematic drawing of mesogen aligned relative to the director, $\hat{n}$ and θ indicates angle for order parameter, S.

Liquid crystal is distinguishable from the liquid phase due to the presence of non-zero degree of ordering. When this order is destroyed, the material becomes isotropic liquid in which all directions are equivalent (no preferred direction). Depending on the shape of the molecules occupying the lattice sites solid can be isotropic or anisotropic (Collings & Hird, 1997). When molecules are spherical or spherical-like, the resulting crystal phase is isotropic (e.g cubic crystal including sodium chloride) and when these are non-spherical, the crystal lattice is anisotropic (e.g graphite) (Guo et al., 2006a; Guo et al., 2006b).

Liquid crystal can be classified into two main groups: thermotropic and lyotropic liquid crystals (Brooks et al., 2011). Thermotropic liquid crystals exhibit phase change by temperature variation while lyotropic phase occur due to temperature variation and suitable solvent and also concentration (Dierking, 2003; Tschierske, 2007). Amphitropic mesogens exhibit both thermotropic and lyotropic liquid crystals (Dierking, 2003; Vill & Hashim, 2002). Brief description of different types of liquid crystals will be discussed below.

1.4.1   Thermotropic Liquid Crystals
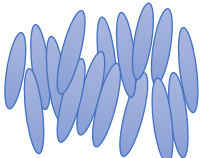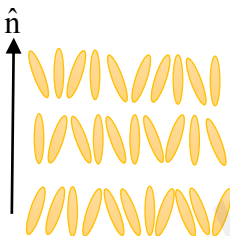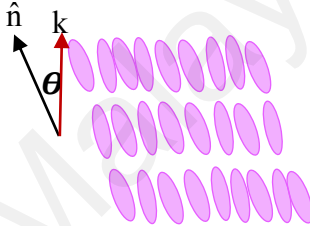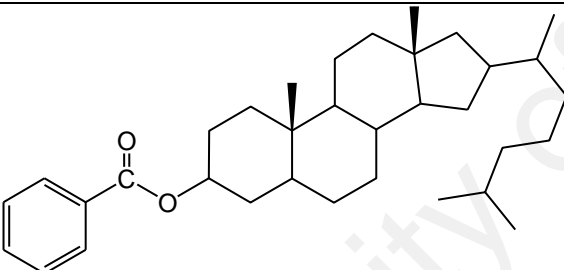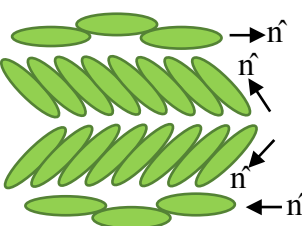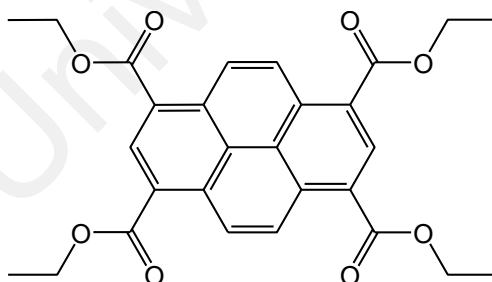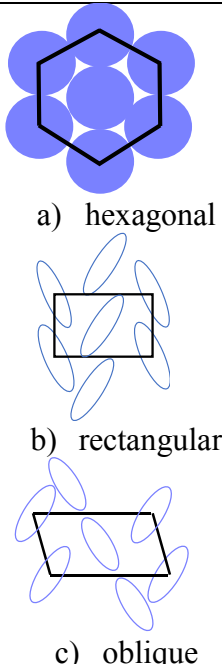
The resulting thermotropic liquid crystalline phase is generally differentiated by the molecular shapes, for examples the calamitic (rod-shaped), discotic (disk-like) and sanidic (brick or lath-like) (Dierking, 2003). The most common type of molecules that form liquid crystal phase is the calamitic or rod-shaped molecules and these give different liquid crystal phases. Some part of the molecules must be rigid to maintain the elongated shape to favour alignment interactions between the long molecular axes (Collings & Hird, 1997). On the other hand, in discotic liquid crystals, which is given by disk-like molecules, the aligning interactions are amongst the short molecular axes. Both calamitic and discotic liquid crystals stable at certain temperature interval are called thermotropic liquid crystals (Collings & Hird, 1997).

The nematic phase of the calamitic liquid crystal is the simplest liquid crystal phase such as 4-butyl-N-[methoxy-benzylidene]-aniline (MBBA) where the molecules only maintain the orientational order without positional order as shown in **Figure 1.9a** (Dierking, 2003).

In some material such as 2,3-difluoro-4-heptyl-4"-pentyl-1,1':4',1"-terphenyl (**Figure 1.9b**), as the temperature decreases the material which is in the nematic phase changes into the Smectic A (*SmA*) and Smectic C (*SmC*) phases. In the *SmA* and *SmC* phases, the arrangement of the molecules exhibit positional order since the molecules centers of mass are arranged in layers with the latter are tilted (**Figure 1.9b**). In the *SmA* phase, the director axis $\hat{n}$ is perpendicular to the normal of the *SmA* layer plane and the orientational order is almost from being perfect as depicted in **Figure 1.9b**. Similar as the *SmA*, *SmC* phase has one degree of (1D) positional order with the director $\hat{n}$ being tilted at an angle θ with respect to layer normal, k (**Figure 1.9b**).

Furthermore, a chiral nematic phase is formed when the molecules exhibit chirality. In chiral nematic phase, the layered structure is tilted by an angle θ of the director $\hat{n}$ which rotates in a helical twist about an axis perpendicular to the director as illustrated in **Figure 1.9c**. This phase is called the cholesteric (*N**) phase (Dierking, 2003).

Discotic liquid crystal includes the nematic and/or the columnar phases, of which the latter can possess order or disorder within the column. Example of compound giving the columnar discotic phase is shown in **Figure 1.9d** from the top view phase (Dierking, 2003). Disk-like molecules form various columnar liquid crystalline phases in the range of the simple nematic to the two-dimensional order of columnar (hexagonal, rectangular and oblique). This type of molecules also form chiral phase when chiral molecules are involved.

Molecular Structure	Phase Behaviour	Type of Phase
H₃CO—⟨benzene⟩—CH=N—⟨benzene⟩—C₄H₉ Cr 22 N 47 Iso (a) 4-butyl-N-[methoxy-benzylidene]-aniline (MBBA)		Nematic (*N*)
C₇H₁₁—⟨difluoro-terphenyl structure⟩—C₅H₁₁ Cr 56.0 SmC 105.5 SmA 131.0 N 136.0 Iso (b) 2,3-difluoro-4-heptyl-4''-pentyl-1,1':4',1''-terphenyl		Smectic A (*SmA*)
		Smectic C (*SmC*)
⟨cholesteryl benzoate structure⟩ Cr* 145 N* 178 BP* 179 Iso* (c) Cholesteryl benzoate		Cholesteric (*N**)
⟨tetraethyl pyrene tetracarboxylate structure⟩ Cr 190 Col 204 Iso (d) Tetraethyl pyrene-1,3,6,8-tetracarboxylate	 a) hexagonal b) rectangular c) oblique	Columnar

Figure 1.9: Mesogen structures and related thermotropic phase structures.

1.4.2   Lyotropic Liquid Crystals (LLCs)
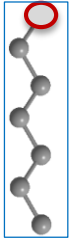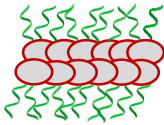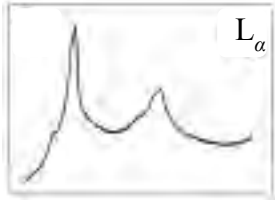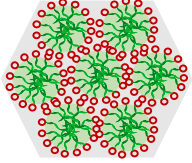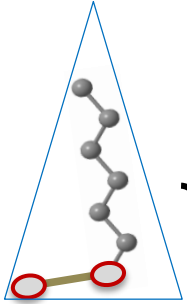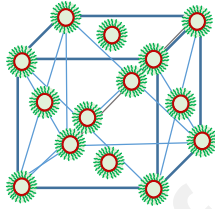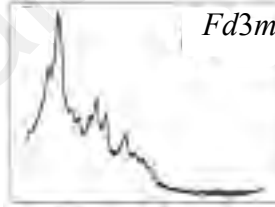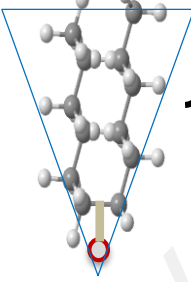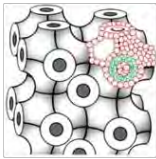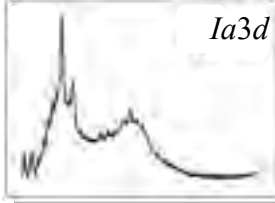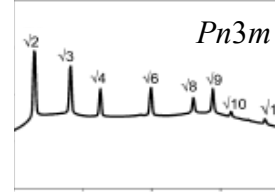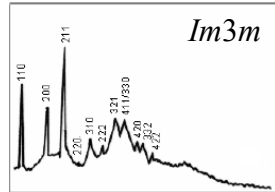
Another category of liquid crystal is the lyotropic liquid crystal (LCC) where the liquid crystal phase appears upon mixing of solvent such as water. Temperature and the concentration factors also play important role to achieve a stable liquid crystal phase. The important feature of molecule forming a lyotropic liquid crystal is the presence of a hydrophilic (water-loving) part at one end with a hydrophobic (lipid-loving) part at the other end of the molecule as depicted in **Figure 1.1**. Thus the molecule is called an amphiphile, i.e. it has a dual tendencies of water loving and water hating. These amphiphilic molecules will form ordered structures in both polar and non-polar solvents, forming a normal phase and an inverse phase respectively (Collings & Hird, 1997). The lyotropic liquid crystal behaviour is widely studied over the whole concentration range. Different solvent concentration gives various of distinct lyotropic liquid crystal phases depending on volume among the hydrophilic and hydrophobic parts, or the hydrophilic lipophilic balance (HLB). The lamellar, hexagonal and cubic phases are common lyotropic liquid crystals and their various structures have been classified by X-ray technique (Collings & Hird, 1997; Guo et al., 2010), see also **Figure 1.10**.

The self-assembly system of lamellar ($L\alpha$) phase is found in double chained and longer chained amphiphiles (Hyde, 2001). Lamellar or neat mesophase structure consists of planar, parallel stacks of amphiphilic bilayer as depicted in **Figure 1.10a**. The polar headgroups are separated by a layer of solvent. Typically, it is called a lamellar mesophase when it exhibits a smectic diffraction pattern and optically anisotropic (Hyde, 2001). In viscosity perspective, lamellar phase is less viscous then hexagonal phase even though containing less water due to its parallel layers that are capable of sliding with ease over each other during shear (Collings & Hird, 1997; Hyde, 2001).

The hexagonal phase comprises of molecular aggregates that corresponds to a hexagonal arrangement as its name implies. This phase has an intermediate viscosity strength compared to micellar and bicontinuous cubic phases (Hyde, 2001). When observed under the optical microscope, this phase has the same birefringent texture as the corresponding columnar thermotropic phase, and is often identified as fan texture due to focal conic domains of columns (Hyde, 2001). Hexagonal lyotropic liquid crystal phase come in two types, which are the normal hexagonal phase (H_I) and the inverse hexagonal phase (H_{II}) as illustrated in **Figure 1.10b**. The hexagonal phase is made up of dense packing of cylinder micelles in a hexagonal arrangement. The inverse hexagonal phase typically has a smaller diameter and obtained at relatively high temperature than the normal hexagonal phase as the non-polar chain may overlap resulting in closer-packed cylinders (Amar-Yuli et al., 2007; Collings & Hird, 1997). The X-ray pattern given by Liew et al. (**Figure 1.10b**) showed H_{II} phase has strong Bragg peaks of $1, \sqrt{3}$ and $\sqrt{4}$ (Liew et al., 2015).

The formation of a cubic phase is not as common as the lamellar or hexagonal phases. They occur in different area of the phase diagram and their position may rely on the molecular structures. They can be produced in the polar chain part (normal phase) or from the non-polar chain part (inversed phase) and the assembly is highly ordered (hence viscous), but is isotropic similar to micelles. For instance, when the monolayer surface curves away from the polar part, it has a positive mean curvature while when this curves towards the polar part, it has negative mean curvature. Therefore, when the surface is planar or parallel stacks, the mean curvature is equal to zero (Liew et al., 2015; Shearman et al., 2006).

Generic Structures	Possible phases	Typical SAXS pattern
	 (a) Lamellar, *Lα*	L_α
	 (b) (i) Normal, *H₁* (ii) Inverse, *H₁₁* Hexagonal	H_{II}
	 (c) Discontinuous Cubic, *Fd3m*	*Fd*3*m*
	 (i) *Ia3d* (ii) *Pn3m* (iii) *Im3m* (d) Bicontinuous Cubic	*Ia*3*d* *Pn*3*m* *Im*3*m*

Figure 1.10: Mesogen structures and related lyotropic phase structures and X-ray pattern (Adopted from (Liew et al., 2015; Sun & Zhang, 2004; Zahid et al., 2013)) of (a) Lamellar (*Lα*) phase, (b) (i) normal hexagonal phase (*H₁*) and (ii) inverse hexagonal phase (*H₁₁*), (c) Discontinuous cubic phase (*Fd3m*) and (d) bicontinuous cubic phase (i) *Ia3d* (ii) *Pn3m* and (iii) *Im3m* (Adopted from (Hashim et al., 2018)).

A discontinuous cubic phase is found when the micellar phase with different sizes and different discrete quasi-spherical micelles packed into cubic structure of specific space group. An example of this cubic phase is *Fd*3*m* as shown in **Figure 1.10c**, which commonly observed ordered micellar phase by being densely packed in a face centered cubic (FCC) lattice (Pouzot et al., 2007; Seddon et al., 2000; Yaghmur & Rappolt, 2013). Liew et al. reported the formation of *Fd*3*m* phase in Guerbet xylose base glycolipids with characteristic peak of SAXS pattern in excess water are $\sqrt{8}$, $\sqrt{11}$, $\sqrt{16}$, $\sqrt{19}$, $\sqrt{24}$, $\sqrt{27}$, $\sqrt{32}$ and $\sqrt{43}$ (Liew et al., 2015; Pouzot et al., 2007).
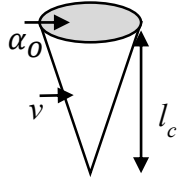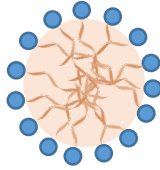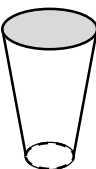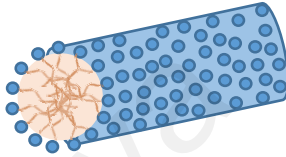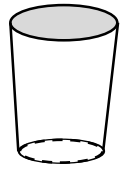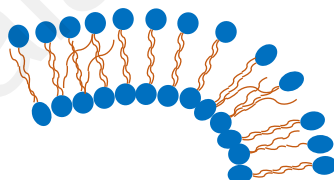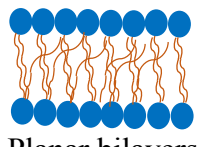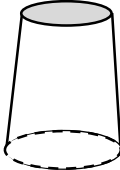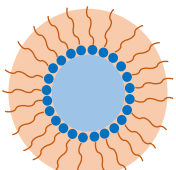
A bicontinuous cubic phase is very viscous, and sometimes nearly solid or rigid and isotropic, thus giving a black optical textures under cross polariser (Hyde, 2001). It originates from a bilayer which is folded on to a triply periodic hyperbolic surface, similar to one of the three homogeneous sponges with zero mean curvature (minimal surface) (Hyde, 2001; Seddon et al., 2000). A bicontinuous cubic phase is normally situated in between the lamellar and the hexagonal phase (Vill & Hashim, 2002). Three common inverse bicontinuous cubic phases have space group of D surface (*Pn*3*m*), G surface (*Ia*3*d*) and P surface (*Im*3*m*) as depicted in **Figure 1.10d** (Hyde, 2001; Seddon et al., 2000a; Seddon et al., 2006b). The X-ray pattern showed in **Figure 1.10d** for *Ia*3*d* (Liew et al., 2015) with spacing ratios of $\sqrt{6}$, $\sqrt{8}$, $\sqrt{14}$, $\sqrt{16}$, $\sqrt{20}$, $\sqrt{22}$, $\sqrt{24}$ and $\sqrt{26}$, while *Pn*3*m* SAXS pattern adopted from (Zahid et al., 2013) and the Bragg peaks displayed in the graph. The *Im*3*m* phase has relative peak positions of X-ray pattern $\sqrt{2}$, $\sqrt{4}$, $\sqrt{6}$, $\sqrt{8}$, $\sqrt{10}$, $\sqrt{12}$, $\sqrt{14}$ and $\sqrt{16}$ (Sun & Zhang, 2004). Among these three cubic phases, *Im*3*m* is less common despite the fact that simplest compared to others (Seddon et al., 2000).

1.5 Critical Packing Parameter (CPP)

Lipid self-assemblies are governed by local constraints and free energy that can be described in terms of the critical packing parameter (CPP) into well-defined structures such as bilayers, micelles and so forth. CPP is defined as **Equation 1.2**

$$CPP = v/\alpha_o l_c \tag{1.2}$$

where v is the volume of the hydrophobic part of the surfactant molecule, α_o is the optimum head group surface area and l_c is the maximum or critical chain length of surfactant tail (Israelachvili, 1994a; Israelachvili et al., 1980b; Israelachvili et al., 1976c). The CPP will identify whether glycolipids will form spherical micelles (CPP<1/3), non-spherical micelles (1/3<CPP<1/2), rod-like micelles (CPP≅1/2), flexible bilayer vesicles (1/2<CPP<1), planar bilayers (CPP≅1) and inversed structures (CPP>1) (Israelachvili, 2011a; Israelachvili et al., 1980b). **Figure 1.11** illustrates the possible structures formed by lipids with different CPP.

Lipid	Lipid Shape	CPP	Resulting Self-assembly
Single-chained lipids with large head group areas	Cone α_O v l_c	<1/3	Spherical micelles
Single-chained lipids with small head group areas	Truncated cone	1/3-1/2	Cylindrical micelles
Double-chained lipids with large head group areas, fluid chains	Truncated cone	1/2-1	Flexible bilayers
Double-chained lipids with small head group areas, anionic lipids in high salt	Cylinder	~1	Planar bilayers
Double-chained lipids with small head group areas, non-ionic lipids, poly (*cis*) unsaturated chains, high temperature	Inverted truncated cone	>1	Inversed micelles

Figure 1.11: Geometries packing properties of lipids and self-assembly structures formed. Redrawn from (Israelachvili et al., 1980).

1.6   Problem Statement

In this research, the hexosomes from Guerbet branched-chain glycolipid were unstable and started to precipitate after 4–7 days (Ahmad et al., 2012). In order to stabilise the hexosomes produced by the technical grade branched-chain glycolipids, the current investigation will use an improved method of hexosome preparation and adding several nonionic co-surfactants from the Tween series (Tween 20 (T20), Tween 40 (T40), Tween 60 (T60) and Tween 80 (T80)) (**Figure 1.12**). Tween series co-surfactants have been applied in many formulations to improve the stability of nanoparticles (Barauskas et al., 2006; Bhattacharya & Dixit, 2015; Shah et al., 2016; Zhao et al, 2010). For example, Zhao et al. have used Tween series (T20 to T80) co-surfactants to improve the stability of the nanoparticles in a system of gold nanoparticles in an aqueous solution (Zhao et al., 2010). Moreover, Barauskas et al. added a small amount of T80 into the mixtures to produce stable sponge phase nanoparticles (Barauskas et al., 2006). Therefore, to improve the nanoparticles's stability, it is common to add the nonionic Tween series surfactants to other surfactant system. From the pharmaceutical point of view, such additives are considered to be safe (Shah et al., 2016). For the current study, Tween series will be added to the branched-chain glycolipid formulation to improve the stability of hexosomes. Physicochemical properties such as critical aggregation concentration (CAC) and particles size of the hexosomes will be determined. A stability analyser will be used to detect any destabilisation of the hexosomes. Thus, this study could contribute to the basic knowledge of branched-chain glycolipid and mixed branched-chain glycolipid-Tween series hexosomes formulation, and thence their use in various applications such as pharmaceutical and cosmetic.
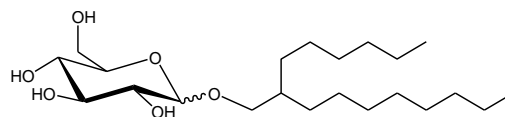
2-hexyldecyl-$\beta(/\alpha)$-D-glucoside ($\alpha\beta$-Glu-OC$_{10}$C$_6$)
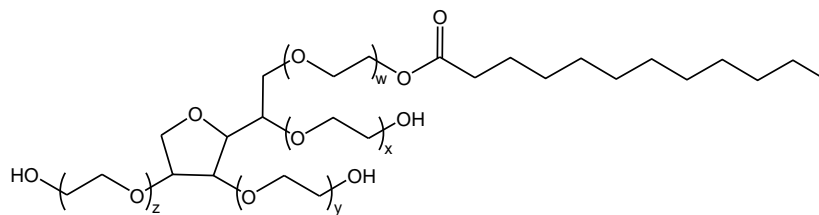
Tween 20 (T20)
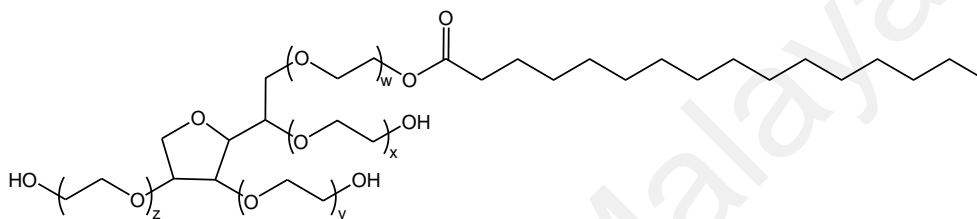
Tween 40 (T40)
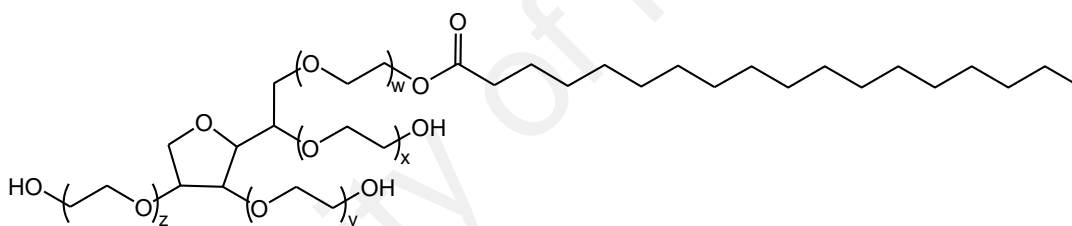
Tween 60 (T60)
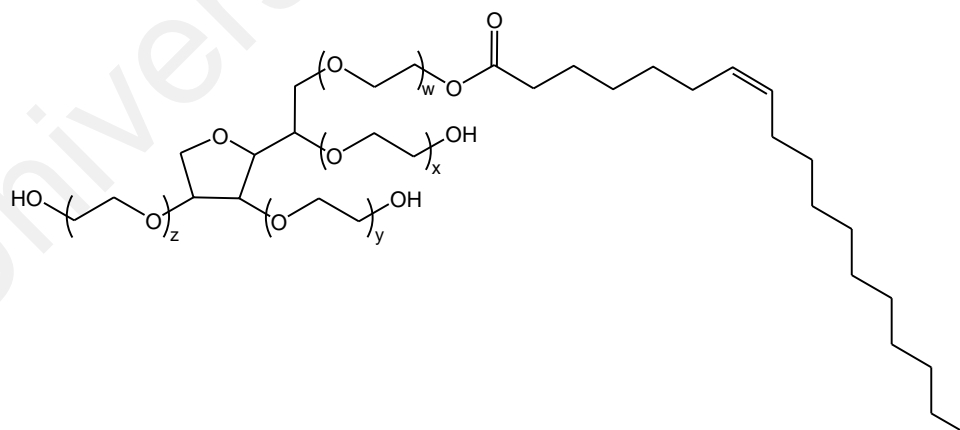
Tween 80 (T80)

Figure 1.12: Chemical structures of nonionic surfactants; $\alpha\beta$-Glu-OC$_{10}$C$_6$ and Tween series (T20, T40, T60 and T80 with alkyl chain lengths of C12, C14, C18 and C18:1, respectively).

19

1.7   Objectives of the Research

The objectives of this research are:

1) To characterise the physicochemical and liquid crystal properties of nonionic branched-chain glycolipid surfactant;

2) To formulate and characterise branched-chain glycolipid nanoparticles and mixed branched-chain glycolipid co-surfactant (Tween series) nanoparticles at room temperature with different compositions; and

3) To evaluate the stability of branched-chain glycolipid nanoparticles and mixed branched-chain glycolipid co-surfactant (Tween series) nanoparticles at different compositions, temperatures and times.

1.8   Dissertation Outline

The dissertation is organised into five chapters. Chapter 1 gives an introduction to the general information of the research by introducing types of surfactant, glycolipids and liquid crystals phases. It also provides problem statement, objectives of the research and dissertation outline. The literature review involves understanding of problems associated with the physicochemical characterisation of nanoparticle and drug delivery system in Chapter 2. Chapter 3 is described the experimental part of the research, sample preparation and the instrumental techniques used to characterise the properties of nonionic branched-chain glycolipid, formulation, and also stability studies of nanoparticles formation which be evaluated in terms of compositions, storage temperatures (25°C and 40°C) and times. Subsequently, in Chapter 4, detail explanation of the results for characterisation of physicochemical and liquid crystalline properties of glycolipids, formulation of branched-chain glycolipid nanoparticles and mixed with nonionic co-surfactant Tween series (T20, T40, T60 and T80) and also stability evaluation are discussed. Finally, Chapter 5 conclude the findings of the research output

and some recommendation for future research works on the application. A list of references and publication paper presented are listed in the dissertation. The appendix is provided in the last part of the dissertation as the supplementary data related to the experimental work.

CHAPTER 2: LITERATURE REVIEW

2.1 Glycolipids Liquid Crystal

Overwhelming trend towards using eco-friendly surfactants has made both synthetic and natural glycolipids a popular option in industry. Due to the problem of purifying natural glycolipids during extraction process, synthetic glycolipids are highly in demand especially when they can reproduce the properties of natural material (Ahmad et al., 2012). Therefore, research and the development of synthetic glycolipids are actively ongoing, supported by the structural improvement of glycolipids to match suitable functional applications. One of the structural improvements for mimicking natural glycolipids is the introduction of chain branching, which has been attempted by many groups (Ahmad et al., 2012; Hashim et al., 2012; Hato et al., 2002; Mannock et al., 2000; Zahid et al., 2013).

Glycolipids are nonionic surfactants but they exhibit different liquid crystalline phases depending on factors such as temperature and concentration (Hashim et al., 2006). Sandoval-Altamirano et al. also reported that the nonionic surfactant glycolipids have widely used in studies of protein purification and membrane solubilisation (Sandoval-Altamirano et al., 2019). Moreover, glycolipids are described as amphitropic (Barón, 2001) because they can form liquid crystals in dry form as well as when in contact with solvents such as water and dimethyl sulfoxide (DMSO) (Ahmad et al., 2012; Blunk et al., 2009; Goodby et al., 2007; Hashim et al., 2011; Nguan et al., 2010; Revathi & Dhanaraju, 2014; Zied et al., 2015).

Glycolipids are also known as polyhydroxy compounds containing sugar groups with many hydroxyl moieties. Hence, these are hygroscopic in nature and it is known that the last trace of water is difficult to remove (Hashim et al., 2018; Loewenstein & Igner, 1991). The extent of dryness in glycolipid is related to the trace water present. The 'dry' octyl-α-glucopyranoside contained less than 0.15 wt% of water and exists as a hemihydrate (Loewenstein & Igner, 1991). Hydration of dry xyloside was investigated where the glycolipid was lyophilised (dry), was left at ambient temperature and also in excess water. It found the water bending mode (*ca.* 1700–1600 cm^{-1}) is negligible for the lyophilised compared to other systems, and this defines 'dry' glycolipid for their system (Hashim et al., 2018; Liew et al., 2015).

The simple packing theory proposed by Israelachvili (Hashim et al., 2012; Israelachvili et al., 1976; Nguan et al., 2010) may suggest the phases (lamellar, hexagonal and cubic) to be observed for these glycolipids. However, an affirmative experimental method such as the various scattering techniques is necessary to confirm the phase structure. Moreover, when the molecule has a small polar head group compared to its chain volume (wedge shape), inverse phases may be obtained (Hyde, 2001; Israelachvili et al., 1980a; Israelachvili et al., 1976b; Nagarajan, 2002; Revathi & Dhanaraju, 2014; Sagnella et al., 2009). Recently, these inverse phases (hexagonal and cubic) draw much interest since they structurally ordered when dispersed into nanoparticles in excess water (Chen et al., 2014). Upon the addition of stabilisers results in the formation of stable colloidal dispersions known as cubosomes and hexosomes (Salim et al., 2015; Thadanki et al., 2011).

Small-angle X-ray scattering (SAXS) is the common method to study the detailed structures of these self-assemblies including inverse mesophases in bulk or dispersed form (**Figure 1.10**) (Sagalowicz et al., 2006). A certain type of self-assembled phase structure and also lattice parameter are determine (position and intensity of the diffraction pattern), although some peaks may be missing or of small intensity due to form factor and strain (Brooks et al., 2011; Sagalowicz et al., 2006; Tyler et al., 2015).

2.2 Hexosome

Hexosome is a colloidal dispersion where elongated rod micelles form an inverse bilayer tubular hexagonal phase, wherein the bulk of it consists of close-packed infinite water cylinder (Siegel, 1986). Upon increasing the water content, the hexagonal phase comprising of cylindrical elements is formed from the breaking up of infinite bilayers (lamellar phase) stacked one over the other in a one-dimensional long-range order structure (Neto et al., 1999). A schematic structure of an inverse bilayer hexagonal phase, H_{II} describes in **Figure 2.1**, where R_P is the phosphate to the center of the water core distance. The bilayer thickness of H_{II}, d_L defines as:

$$d_L = a - 2R_W \tag{2.1}$$

where a is the unit cell parameter of the H_{II} and R_W is the radius of the water core. In H_{II}, Rappolt et al. were reported that H_{II} of 1-Palmitoyl-2-oleoyl-sn-phosphatidyl-ethanolamine (POPE), where R_W inside the tubes is much larger than the bilayer of separation in the lamellar phase of POPE (30 Å ≥ 5 Å) and difference in bilayer thickness, d_L is only ~3 Å (Rappolt et al., 2003). The H_{II} phase structure consists of tubular of water arranged on hexagonal lattice.

The illustration of bilayer inverse hexagonal phase as showed in **Figure 2.1**. The lipid monolayer is enveloping around each water core (light blue region represent water) with polar headgroup of lipid molecule at the water interface and nonpolar hydrocarbon tail fill the interstitial space of the lattice (Galliková et al., 2018; Perutková et al., 2011; Rappolt, 2006; Tate & Gruner, 1989). Perutkova et al. also reported that not all the hexagonal lattice of lipid hydrocarbon tails has same length (Perutková et al., 2009). Furthermore, using phytantriol/ Pluronic F127 and 10% w/w of decyl betainate chloride (DBC), Ribeiro et al. reported that alkyl chains in the bilayer are interdigitated because hydrophilic headgroups of bilayer comprises of phytantriol, Pluronic F127 and also DBC, while hydrophobic tails consist of phytantriol and DBC (Ribeiro et al., 2019). The interdigitated structure influence by increasing the strength of repulsive interaction between the polar headgroups, Lu and coworker reported that lipids with larger polar group (eg. phosphatidylcholines, PC) generally sub-transition into gel phase where hydrocarbon tails collectively tilted (Lu & Guo, 2018). For short lipid tails it touch across lattice space, however their density is low in between the bilayer, while for long lipid tails severely constrained from normal to bilayer plane, and thus splay to this plane and high density packing in the middle of bilayer (Nielsen et al., 2004). The ability of bilayer structure to encapsulate the polar, non-polar and also dual properties of macromolecule in H_{II} phase.
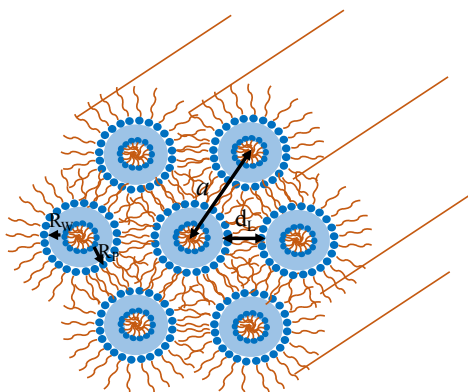
Figure 2.1: A schematic structure of an inverse hexagonal phase, H_{II}.

This H_{II} structure allows the macromolecule has dual characters such as DNA, enzyme and also protein which can be fitted. Therefore, H_{II} phase have great attraction in the research area, because they can form complexes with DNA. It can mimic natural viruses in the ability to act as synthetic carrier of cellular DNA for gene delivery across outer cell membrane (Galliková et al., 2018; Sum et al., 2014; Koltover et al., 1998).

Furthermore, oleyl glycerate (OG) and phytanyl glycerate (PG) also give hexagonal phases. This glycerate is potentially useful as drug carrier system (Guo et al., 2010). For example, Hirlekar et al. study in pharmaceutical application, biologically active molecules can either be adjusted within the aqueous domains or can be directly coupled to the lipid hydrophobic moieties oriented radially outwards from the centre of the water rods. Due to these special properties of hexosomes, they are used to improve the solubility of poorly water soluble drugs and to transport therapeutic peptides and proteins by oral, transdermal, and parenteral routes (Hirlekar et al., 2010).

Hexagonal lyotropic liquid crystals have been extensively studied by many groups to produce hexosome delivery systems. Neto et al., have used imaging soft matter with atomic force microscope (AFM) to study hexagonal phase of 97% wt of water, using GMO/GTO and Polaxamer 407 in certain proportion. System of GMO/GTO in the ratio of 88/12 produces hexosomes on mica with an average size of 150 nm (Neto et al., 1999). On the other hand, Yuli et al. found the formation of hexosomes mediated using hydration and stabiliser (polymeric). Their system contains GMO/tricaprylin/water and stabiliser Pluronic F127 and they obtained a small and more stable soft particle with high symmetry of hexosomes. However, when polymer stabiliser is less (<1.0 wt%), only partial polymer adsorption occurs during dispersion process and insufficient of this adsorption lead to less ordered hexosomes of lower stability and larger size (Amar-Yuli et al., 2007).

Furthermore, by using phytantriol: Pluronic F127 in a composition of 9:1 mass ratio, Boyd et al. (Boyd et al., 2007) reported that hexosomes are not necessarily flat hexagonal prisms. Hexosome images obtained by Cryo-TEM provides the hexagonal shaped silhouette. When using Cryo-FESEM with spinning top a 3D structure is produced while on the upper surface a spine structure is observed. Therefore, no flat hexagonal prism structures are observed in Cryo-FESEM images of H_{II} phases (Boyd et al., 2007). Topical vehicles of peptides using hexosomes drug delivery system containing nanodispersion of monoolein and oleic acid was reported by Lopes et al. (Lopes et al., 2006). The lipid composition of this mixture contains monoolein/oleic acid/poloxamer 407/water and a bioactive ingredient Cyclosporin A (CysA) was assessed *in vitro* and *in vivo*. The hexosome's diameter was 181.77 ± 1.08 nm and at 0.6% of lipids mixture, CysA did not change the liquid crystalline structure (Lopes et al., 2006). Other study of hexosomes in oromucosal delivery found this phase formulation exhibited high permeability, high entrapment efficiency and better stability of storage, resulting in enhanced delivery of the active ingredient (progesterone) (Swarnakar et al., 2007). A summary of current applications of lyotropic liquid crystals (LLCs) as delivery systems reported in **Table 2.1**.

An inversed hexagonal (H_{II}) phase was reported by Brooks et al. using nonionic Guerbet branched-chain β-D-glucosides in dry and excess system. In dry system, the longer chain lipids (β-Glu-: $C_{14}C_{10}$, $C_{12}C_8$ and C_{10},C_6) form inversed hexagonal (H_{II}) phase, while in excess system, β-Glu-$C_{12}C_8$ showed H_{II} phase and β-Glu-$C_{14}C_{10}$ at 25ºC form $L\alpha$ phase but upon heating at 48ºC its form H_{II} phase (Brooks et al., 2011). Liew et al. also used same Guerbet surfactant as Brooks et al. study, however different in sugar group which is xylose. The thermotropic conditions, xylose with C_{16}, C_{20} and C_{24} form H_{II} phases, whereas hydration conditions, only xylose with C_{16} and C_{20} remain in H_{II} phase while C_{24} forms $Fd3m$ cubic phase (Liew et al., 2015). Previously, technical grade

(anomeric mixture containing 10% α anomer) β-anomer of Guerbet branched-chain

glycolipid was studied (Ahmad et al., 2012). When observed under optical polarising

microscope (OPM) and SAXS, this Guerbet branched-chain glycolipid formed an inverse

hexagonal phase. Additionally, a partial phase diagram of Guerbet branched-chain

glycolipid has been constructed and a two-phase region has shown the formation of the

inverse hexagonal phase. This hexagonal phase was used to prepare hexosomes using top

down approach (Chen et al., 2014; Guo et al., 2010).

Table 2.1: Lyotropic liquid crystals mesophase as delivery systems reported in year 2005-
2017.

Type of lyotropic liquid crystals (LLCs)	Lipid system	Boactive molecule	Administration route	Refs
Cubic bulk phase, Hexagonal bulk phase	GMO/water, PT/water, PT/VitEA/water	Glucose, Allura Red, FITC-dextran	Oral administration	(Lee et al., 2009)
Hexagonal bulk phase	OG/water	Sodium pamidronate	Oral administration	(Boyd et al, 2005)
Cubic bulk phase, Hexagonal bulk phase	GMO/water, GMO/oleic acid/water	Cys A	Topical application	(Lopes et al., 2006)
Hexosomes	GMO/oleic acid/F127/water	Cys A	Topical application	(Lopes et al., 2006)
Hexagonal bulk phase, Hexosomes	GMO/water, GMO/F127/water	Vit K	Topical application	(Lopes et al., 2007)
Hexosomes	GMO/oleic acid/F68/water	Progesterone	Mucosal application	(Swarnakar et al., 2007)
Hexagonal bulk phase	GMO/oleic acid/F127/water	Rosuvastatin	Oral administration	(Gabr et al., 2017)

Type of lyotropic liquid crystals (LLCs)	Lipid system	Boactive molecule	Administration route	Refs
Hexagonal phase gel	GMO/TAG/water	Sodium diclofenac	Transdermal administration	(Cohen-Avrahami et al., 2010a; Cohen-Avrahami et al., 2012b)
Cubic bulk phase, Hexagonal bulk phase	Phyt/water/ Cinnarizine, Phyt/water/ Diazepam, Phyt/water/VitEA	Cinnarizine, Diazepam, VitEA	Oral administration	(Nguyen et al., 2011)
Cubic bulk phase, Hexagonal bulk phase	Phyt/water/glucose Phyt/water/VitEA/ glucose	Glucose	Subcutaneous	(Fong et al., 2009)
In situ cubic phase/in situ hexagonal phase	Phyt/water/ethanol/ SMH, Phyt/water/ethanol/ VitEA/SMH	Sinomenine hydrochloride (SMH)	Intra-articular	(Chen et al., 2015)
Cubosomes, Hexosomes	GMO/ F127/water Phyt/F127/water Phyt/F127/water/ VitEA	Dichlorodiphenyldichloroethylene (DDE)	Agrochemical application	(Dong et al., 2011)

CHAPTER 3: METHODOLOGY

The synthesis of anomeric mixture of 2-hexyldecyl-$\beta(/\alpha)$-D-glucoside ($\alpha\beta$-Glu-OC$_{10}$C$_6$) followed by the well-established procedures of peracetylation, glycosidation, and deacetylation. The synthesis of $\alpha\beta$-Glu-OC$_{10}$C$_6$ only involve two parts; glycosidation and deacetylation stages, as peracetylation was not carried out due to the β-D-glucose pentaacetate is being commercially and readily available. The use of peracetylated sugar and alkyl chain of the Guerbet alcohol in the presence of catalyst boron trifluoride diethyl etherate forms the core of the glycosidation step. The final step of deacetylation involves the removal of the acetate group in the intermediate product by dissolving the compound in methanol and sodium methoxide (Hashim et al., 2006).

3.1   Materials

The anomeric mixture of 2-hexyldecyl-$\beta(/\alpha)$-D-glucoside ($\alpha\beta$-Glu-OC$_{10}$C$_6$) was synthesised using a procedure reported by Hashim et al. (Hashim et al., 2006). Since the product was an anomeric mixture, its purity was ~90% β, as per to ^{1}H NMR (see **Appendix A**). In this work, the anomeric mixture $\alpha\beta$-Glu-OC$_{10}$C$_6$ is also referred as "technical grade", since it was produced by avoiding the complex column chromatography procedure for the extraction of only β anomer, rendering the anomeric mixture ~10% α anomer. The $\alpha\beta$-Glu-OC$_{10}$C$_6$ was extensively dried prior to characterisation by placing the glycolipid in a vacuum oven over phosphorus pentoxide for more than 24 h. The nonionic surfactant Tween series: Tween 20 (T20), Tween 40 (T40), Tween 60 (T60), and Tween 80 (T80) were purchased from Sigma-Aldrich. Sample preparations utilised deionised water produced from Diamond Nano-pure deioniser, reporting an ionic conductivity of 18.2 μS/cm.

3.2   Thermogravimetric Analyser (TGA)

Thermogravimetric analyser (TGA) is a quantitative measurement that can be used to determine the weight change of samples as a function of increasing temperature. The weight of the sample can be determined using a thermobalance (Van Gestel, 2007). The measurement is usually performed under inert atmospheres such as nitrogen, helium or argon, or oxidative ones such as oxygen/air (Menczel et al., 2009). It can be used to obtain the information on absorbed moisture/impurities in the sample and also its decomposition temperature.

The important part of the TGA is its thermobalance, which measures the weight of sample as a function of temperature and time. Also, TGA is a complementary tool to DSC for determining the decomposition temperature of materials. There are several factors that can affect TGA measurements, such as atmospheric turbulence, electrical considerations, and secondary reactions. However, these negative effects can be mitigated by carrying out a second experiment using an inert sample, controlling the temperature of the balance chamber, and optimising atmospheric flows (Menczel et al., 2009).

3.2.1   Sample Preparation

The $\alpha\beta$-Glu-OC$_{10}$C$_6$ sample was dried extensively prior to characterisation by placing the glycolipid in a vacuum oven over phosphorus pentoxide for more than 24h, as per **Section 3.1**. ~10 mg of a dry $\alpha\beta$-Glu-OC$_{10}$C$_6$ was placed onto an aluminum pan.

3.2.2 Measurement

TGA measurement was performed using a Perkin Elmer TGA 4000 (Massachusetts, USA). The sample was examined at 45-500°C, at a heating rate of 10°C min^{-1}. Analysed data was refined using Pyris Series software and plotted as a thermogram of weight percent as a function of temperature.

3.3 Differential Scanning Calorimetry (DSC)

Differential scanning calorimetry (DSC) is a quantitative direct measurement method (O'neill, 1966) that can be used to determine the difference of heat flow rate of samples and its reference as a function of temperature throughout the temperature program (Menczel et al., 2009; Van Gestel, 2007). DSC is especially useful when samples are quantitatively inadequate, due to its measurement requirement being only a few mg of sample. DSC measures the amount of heat absorbed from the surroundings (endothermic process) or heat released to the surrounding (exothermic process) during heating/cooling (Collings & Hird, 1997).

Sample undergoes a phase transformation when heated, and subtle phase changes evident in DSC plots represents enthalpy changes. DSC is especially important in the context of optical polarising microscope (OPM) confirming the presence of mesophase from phase changes due to enthalpy gradient. Although this technique cannot be used to determine the type of liquid crystalline phases, it can provide information on the degree of molecular ordering of mesophase via levels of enthalpy changes (Collings & Hird, 1997).
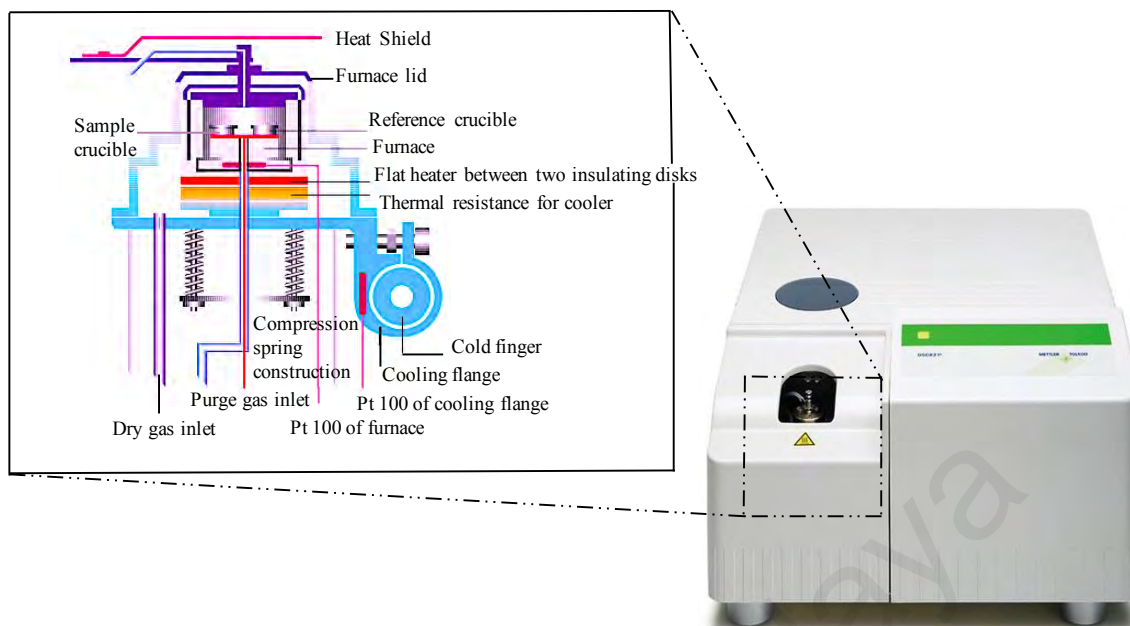
Figure 3.1: Setup of a differential scanning calorimeter. Redrawn from (Van Gestel, 2007).

3.3.1 Sample Preparation

The $\alpha\beta$-Glu-OC$_{10}$C$_6$ sample was dried as per the steps outlined in **Section 3.1**. ~5-10 mg of $\alpha\beta$-Glu-OC$_{10}$C$_6$ sample was encapsulated into an aluminum pan and crimp-sealed with a lid to ensure excellent thermal contact. The lid is also expected to press down on the sample as much as possible to create a compact and airtight seal (Menczel et al., 2009).

3.3.2 Measurement

Phase transition with respect to temperature(s) was performed using a Mettler Toledo DSC 822^e equipped with Haake EK90/MT intercooler, as per **Figure 3.1**. An empty aluminum pan was used as a reference, and the DSC was calibrated using standard indium for temperature and enthalpy accuracy prior to measurement. The measurement was conducted from -25-150°C at a scanning rate of 5°C min^{-1} after loading the sample into the DSC. The data was then analysed with STARe Thermal Analysis System software, and plotted as heat flow as a function of temperature.

3.4 Optical Polarising Microscope (OPM)

Optical polarising microscope (OPM) is one of the essential tools for both quantitative and qualitative measurements at an anisotropic phase (Robinson & Davidson, 2016). It can also provide a phase transition temperature and identify the liquid crystalline phase of a sample (Goodby, 2014). The polarising microscope technique is able to distinguish between isotropic and anisotropic media at a glance. **Figure 3.2** illustrates a typical setup of an optical polarising microscope.

Figure 3.2: A schematic setup of an optical polarising microscope. Redrawn from (Robinson & Davidson, 2016).

The microscope is equipped with both cross-polariser, where the first polariser is positioned in the light path somewhere before the sample, and another is placed in the optical pathway between the objectives and camera port. Due to the fact that the polarisers are perpendicular to each other within the microscope, if an isotropic liquid is analysed then polarised, it remains unaffected by the sample, therefore, no light passes through the second polariser. Similarly, when an anisotropic sample is present, it results in birefringent, where the light is not extinguished and an optical texture provide distinct

liquid crystal (Collings & Hird, 1997). Image contrast from the interaction of plane-polarised light with a birefringent (doubly-refracting) produces two wave components that are each polarised in mutually perpendicular planes. The light components go out of phase after exiting the sample, but recombines with constructive/destructive interferences when passing through the analyser (Robinson & Davidson, 2016). The optical polarising microscope is the broadest tool of study for analysing thermotropic/lyotropic behaviours.

3.4.1 Thermotropic Behaviour

The thermotropic analyses in this study involved placing a small amount of dried $\alpha\beta$-Glu-OC$_{10}$C$_6$ sample onto a clean glass slide and covering it with a slip, as shown in **Figure 3.3**. The slide was then launched onto a temperature-controlled microscope slide holder, and subsequently placed on the microscope's stage. The sample was heated then cooled twice prior to the measurement. First, the sample was heated until it reached its isotropic phase to eliminate any trapped moisture in the sample and to form a thin film of glycolipid on the slide. The cover slip was gently pressed while heated to produce a uniform layer in order to obtain a better texture. Then, the sample was slowly cooled to 25°C prior to being heated again. The texture was recorded when cooled at a rate of 1°C min^{-1}.
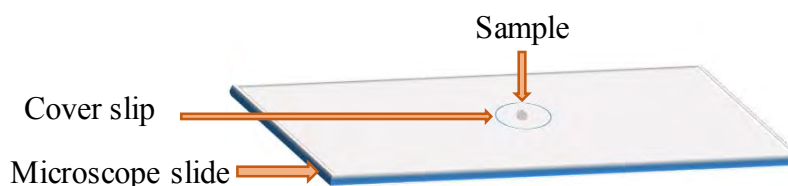
Figure 3.3: Preparation of OPM sample for thermotropic study.

3.4.2   Lyotropic Behaviour

The contact penetration experiment was used to identify the formation of liquid crystalline phases in the presence of water. Water was used due to its compatibility with biological systems and also the fact that it is a common polar solvent used in the formulation of the delivery system (Ahmad et al., 2012; Hashim et al., 2012; Hato et al., 2002; Mannock et al., 2000; Zahid et al., 2013). Water is also capable of forming H-bonds with the hydroxyl group in glycolipids and provides a high cohesive-energy density that stabilises the mesophases. A neat surface of sample was prepared on a clean microscope slide and covered with a cover slip. The sample was heated up to its isotropic phase then cooled to room temperature. A drop of deionised water was placed at the edge of the cover slip (**Figure 3.4**), and water penetrates via capillary forces into the sample, from deionised water to the neat surfactant. The solvated sample was then studied under polarised light, and its textures represents the type of liquid crystalline phase present.
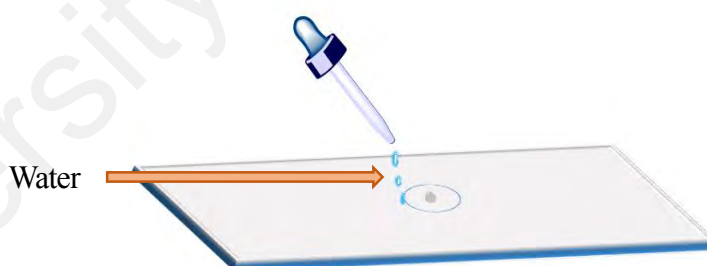
Figure 3.4: Contact penetration technique for lyotropic system.

3.4.3   Measurement

The liquid crystal phase of the $\alpha\beta$-Glu-OC$_{10}$C$_6$ sample was identified using an optical microscope (Olympus BX51, Tokyo, Japan) equipped with cross-polarising filters and a Mettler Toledo FP82HT hot stage. The microscope is also equipped with a temperature controller (FP90 Central Processor), and was connected to a camera (Olympus DP26) for image capture. Captured images were analysed using the cellSans software. The images were captured in the presence of cross-polarising lenses at 4x, 10x, 20x, or 50x magnification factors depend on the quality of image.

3.5   Small-angle X-ray Scattering (SAXS)

The X-ray scattering technique is a non-destructive technique that can be used to discern the structure and elastic parameter of fluid bilayers (Pabst et al., 2010; Tyler et al., 2015). Small-angle region of the scattering pattern in SAXS exhibits long range order of the structure and symmetry specify the phase of lyotropic liquid crystal (LLC) (Tyler et al., 2015). SAXS is a powerful tool that can be used to determine the size, shape, distribution, and positions of nanoparticles (Allec et al., 2015; Londoño et al., 2018). It can even be used to define the texture of thermotropic and lyotropic liquid crystallines. SAXS is able to discern information pertaining to the structures measuring 0.5-100 nm, depending on its experimental setup. Limitations of this technique involve its X-ray beam, range of sample to detector, size and geometry of detector, and beam stopper sizer, as per **Figure 3.5** (Craievich, 2018; Londoño et al., 2018).
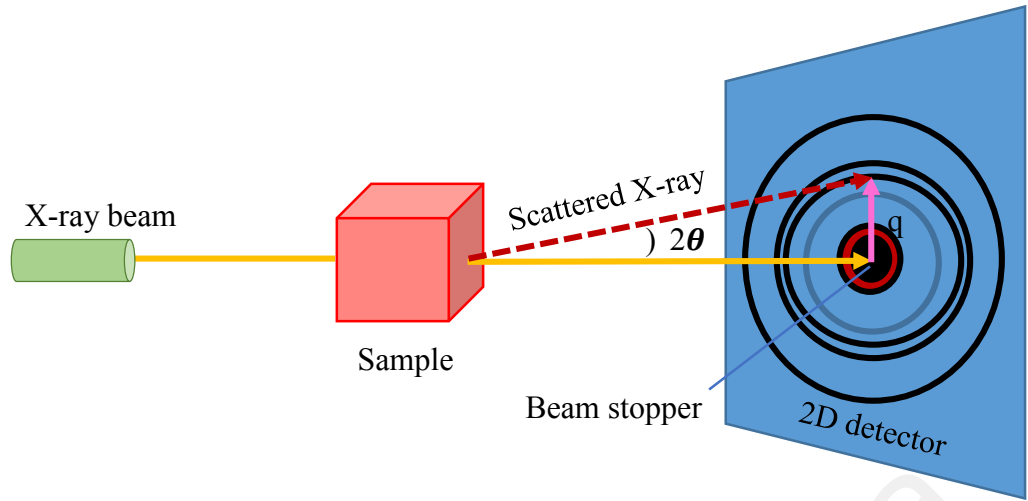
Figure 3.5: A schematic diagram of SAXS setup. Redrawn from (Londoño et al., 2018).

To understand how the X-ray scatter at lower angles, its visualised using Bragg's law, as shown in **Equation 3.1** and **Figure 3.6**, where the incident wavelength is scattered by the discrete, parallel plane in the crystal separated by distance, d

$$\eta\lambda = 2d_{hkl}\sin\theta \qquad (3.1)$$

where η is the order of reflection, λ is the wavelength of X-ray radiation, θ is the scattering angle between the scattered X-ray and the plane formed by the sample surface, 2θ is the scattering angle between incident and scattered X-ray and d_{hkl} is the distance between repeating planes in the lattice (Svergun et al., 2013).
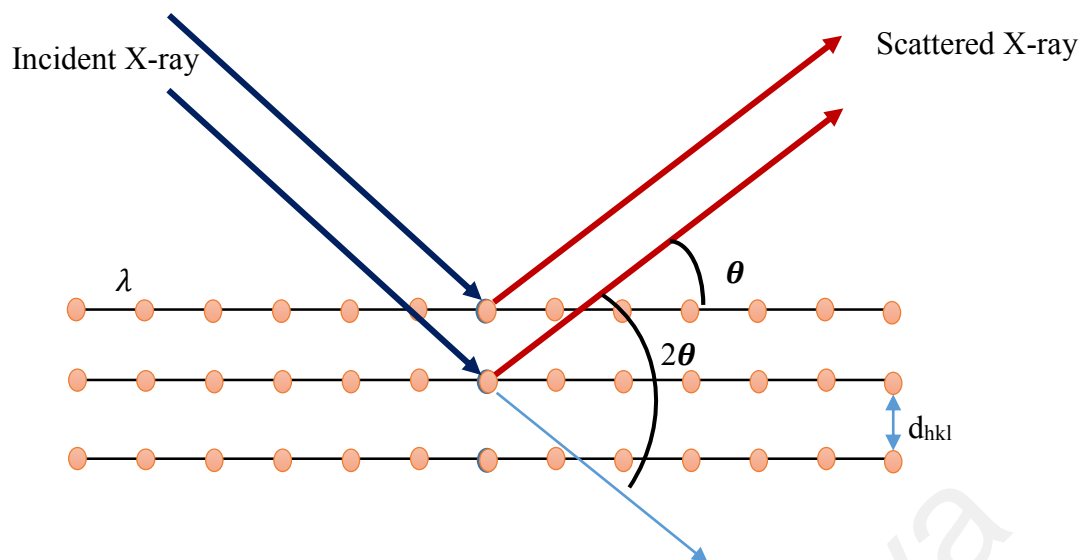
Figure 3.6: A schematic drawing illustrates the Bragg's Law.

3.5.1 Sample Preparation

Prior to the day of measurement, the dried sample was stored in a vacuum desiccator for 24 h. The sample (~50 mg) was transferred onto a paste cell holder and placed into the X-ray machine. The 95% water sample (hydrated $\alpha\beta$-Glu-OC$_{10}$C$_6$) was prepared by adding 1.0 mL of deionised water to the 50.0 mg of $\alpha\beta$-Glu-OC$_{10}$C$_6$ and heated at 65°C for 30 mins. Prior to the SAXS measurement, the hydrated sample was equilibrated for at least three days.

3.5.2 Measurement

The small-angle X-ray scattering experiments were carried out for both dried and hydrated samples using SAXSess from Anton Paar, Austria. This instrument was equipped with an X-ray tube (DX-Cu 12x0.45, SERFERT) generator producing Cu-Kα radiation at wavelength, λ = 1.542 Å and operating at 40 kV and 50 mA. Silver behenate (λ = 58.4 Å) was used for calibration. An acquisition time of 1 h was applied for both dried and hydrated samples at multiple temperatures (25°C, 40°C, 60°C, 80°C and 100°C).

The data were analysed using SAXSquant software while liquid crystal phases were assigned using the SGI software.

3.6   Tensiometer

The critical aggregation concentration (CAC) is the minimum concentration where the formation of molecular aggregates is detectable. The surface tension of CAC is found to be lower than critical micellar concentration (CMC) of surfactant solution (Diamant & Andelman, 1999), which corresponds to the onset of micelle formation on the surfactant, as shown in **Figure 3.7.** The addition of more surfactants to the solution results in it being saturated with surfactant micelles, and then the monomer surfactant concentration begins increasing, which decreases the surface tension to under the plateau region shown in **Figure 3.7** until the monomer surfactant form free micelles (Sekhar et al., 2019; Taylor et al., 2007)
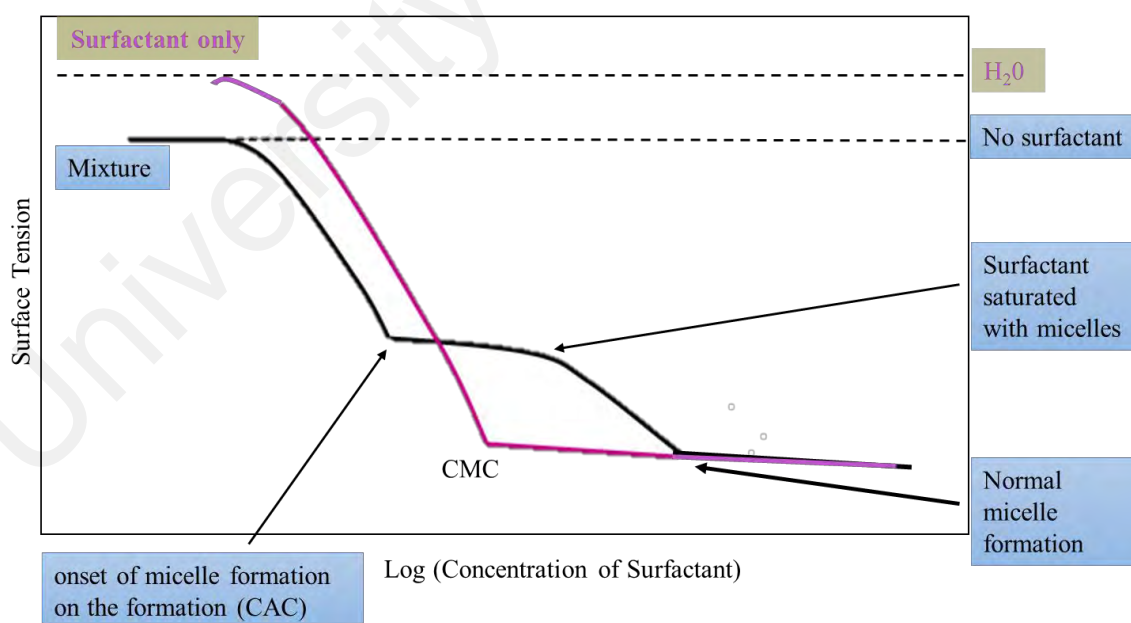
Figure 3.7: Surface tension behaviour of surfactant mixtures.

3.6.1   Sample Preparation

Critical aggregation concentrations (CACs) of the nonionic branched-chain glycolipid sample and mixed surfactants system of branched-chain glycolipid with other nonionic surfactants (Tween series: T20, T40, T60 and T80) were analysed in an aqueous media at 25°C. Several different formulations ratios were tested in the preliminary study, where an optimised ratio of 10:1 of branched-chain glycolipid to Tween series was selected as a stock solution. The stock solution was then diluted to prepare a series of solution at different concentrations for CAC measurement.

3.6.2   Measurement

The surface tension technique was used in this study to measure the aggregation behaviour of branched-chain glycolipid with and without the addition of co-surfactants. A KSV Sigma 702 Tensiometer from Finland (**Figure 3.8**) was utilised to determine the critical aggregation concentration (CAC). The measurements were conducted for a nonionic glycolipid surfactant and mixed surfactants system of glycolipid with other nonionic surfactants i.e. T20, T40, T60 and T80 in an aqueous solution at 25°C. Prior to the measurement, the platinum ring was cleaned using acetone and washed thoroughly with deionised distilled water, then burnt red using a Bunsen burner. Since the Du Nouy Ring method was used, calibration with deionised distilled water was required prior to the measurement. The surface tension for deionised distilled water is fixed, at ~71-72 mN/m. The CAC values are obtained from a conventional plot of the surfactant's surface tension versus the log of its concentration. On this plot, the CAC corresponds to the point of the lowest surface tension before it remains relatively constant beyond this point.
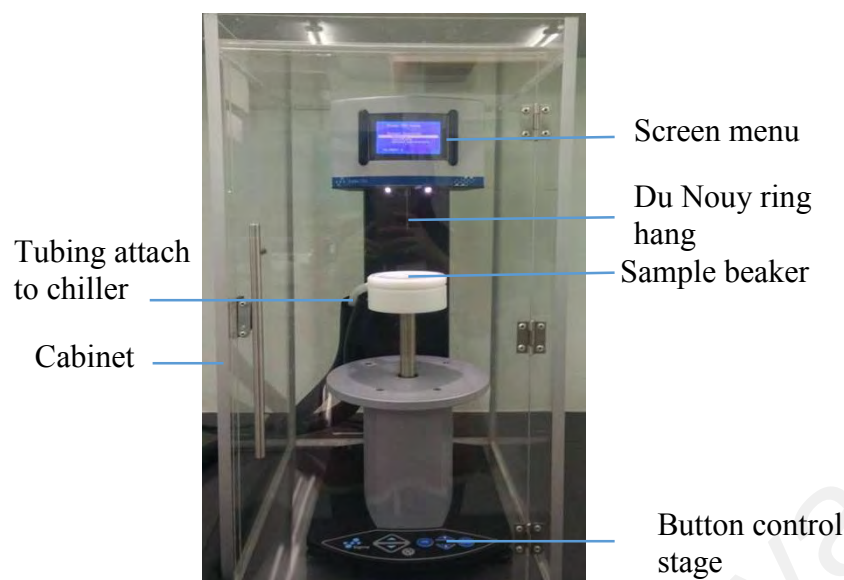
Figure 3.8: Setup of a tensiometer.

3.7 Hexosomes Preparation

The $\alpha\beta$-Glu-OC$_{10}$C$_6$ dispersion in water was equilibrated for three days, then sonicated for 30 min in a water bath at 70°C and heated for 2 h at 80°C. The $\alpha\beta$-Glu-OC$_{10}$C$_6$ sample was passed through an N$_2$-driven extruder (10 mL Lipex, Northern Lipids Inc.) with polycarbonate filters with pore size is 100 nm. This was done for more than 10 cycles to acquire small size hexosomes with a homogeneous size distribution. The same procedure was applied to mixture solutions of branched chain glycolipid:Tween series (T20, T40, T60 and T80) at the ratio of 10:1 of branched-chain glycolipid:Tween series.

3.8   Particle Sizer - Dynamic Light Scattering (DLS)

The dynamic light scattering (DLS) method measures the average hydrodynamic size and polydispersity of particles based on Brownian motion of dispersed particles (Berne & Pecora, 2000; Burchard, 1983; Pecora, 2013). When particles are dispersed, they move freely in all directions. The principle of Brownian motion is the random movement of particles due to the particles colliding with solvent molecules. The energy transfer is almost constant, which translates into more significant effect on smaller particles. Smaller particles experience more pronounced Brownian motion in this case.

3.8.1   Measurement

Dynamic light scattering (DLS) experiments were conducted using Zetasizer nano-ZS (Malvern) equipped with a 633 nm He-Ne laser light source (**Figure 3.9**). DLS was used to determine the average hydrodynamic size and distribution of hexosomes from branched-chain glycolipid sample and those of mixed branched-chain glycolipid:Tween series hexosomes at 25°C.
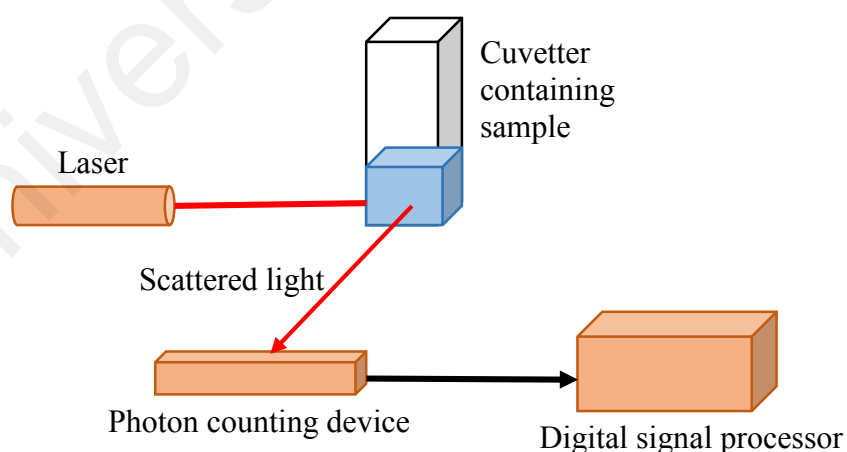
Figure 3.9: Basic setup of DSL measurement.

3.9   Transmission Electron Microscope (TEM) Determination

The morphology of the branched-chain glycolipid sample and mixed branched-chain glycolipid-Tween series hexosomes were determined using Transmission Electron Microscope (TEM, HF-3300 TEM/STEM combines cold field emission gun (CFEG) operating at 300 kV accelerating voltage). 10 μL of the branched-chain glycolipid sample and mixed branched-chain glycolipid:Tween series hexosomes samples were placed on a carbon-coated copper grid and the excess samples were completely removed after 10 mins of incubation. The samples were then stained by adding 5 μL of 1% (w/v) phosphotungstic acid solution, followed by 5 min incubation and excess solution removal.

3.10   Stability Determination

Stability is a key issue when developing new formulations using hexosomes samples. Backscattered (BS) light and dynamic light scattering (DLS) methods are often used to study the stability of suspensions or emulsions and estimate the dispersed phase properties such as particle size. The BS light can be measured by Turbiscan analysis, which provides information about the destabilisation phenomena. This could be due to particle migration (sedimentation or creaming) and particle size variation (flocculation or coalescence) (Buron et al., 2004; Mengual et al, 1999a; Mengual et al., 1999b; Tan et al, 2015). There are few benefits to the Turbiscan analysis; it is able to detect destabilisation much earlier than the naked eye, especially in concentrated and opaque systems, it is non-destructive (no sample dilution), and it can also measure irreversible processes such as flocculation/coalescence and reversible processes such as sedimentation/creaming without requiring sample dilution (Celia et al., 2009; Lemarchand et al., 2003a; Lemarchand et al., 2003b).

3.10.1 Stability Analyser - Backscattered (BS) Light

The Turbiscan Classic MA 2000 Stability Analyser (Formulaction SA., France), equipped with an 850-nm laser, is shown in **Figure 3.10**. The stability of the branched-chain glycolipid sample and those from mixed branched-chain glycolipid-Tween series hexosomes were investigated to detect destabilisation of the systems correlate with particles size variations and particles migration. The measurement of the Turbiscan stability analyser are based on multiple light scattering method, where a sample in a 60 mm standardized cell is scanned as a function of sample height for 24 h in the backscattering mode at room temperature.
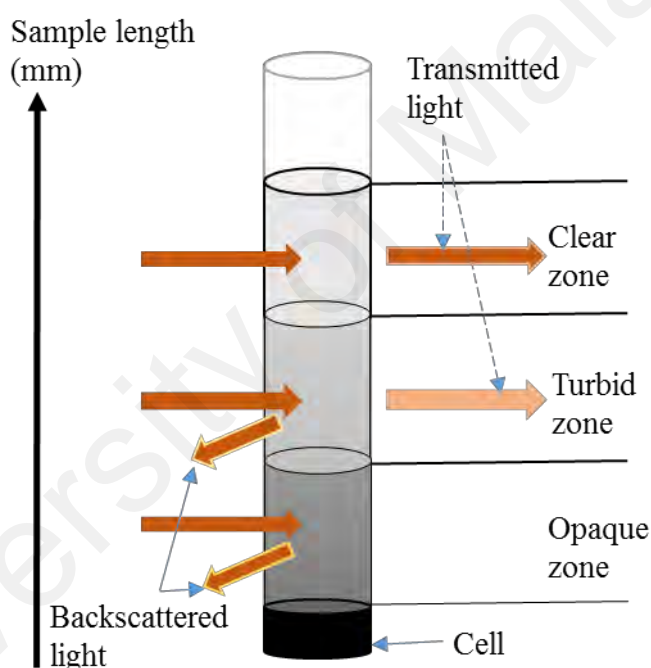
Figure 3.10: Turbiscan measurement principle.

3.10.2 Particle Sizer - Dynamic Light Scattering (DLS)

The stability of the branched-chain glycolipid sample and mixed branched-chain glycolipid-Tween series hexosomes were analysed at two different temperatures of 25°C and 40°C for a month. The particles sizes of the hexosomes were determined using the DLS method.

CHAPTER 4: RESULTS AND DISCUSSION

This chapter will focus on the results and discussion of the present studies. In this research, the liquid crystalline and self-assembly properties of a novel branch alkylated glycolipid, namely 2-hexyldecyl-$\beta(/\alpha)$-D-glucoside ($\alpha\beta$-Glu-OC$_{10}$C$_6$), was synthesized using a procedure as mentioned in the Chapter 3 by Hashim and co-workers (Hashim et al., 2006). To be consistent with the previous work and to guarantee reproducibility (Ahmad et al., 2012), the $\alpha\beta$-Glu-OC$_{10}$C$_6$ was extensively dried prior to any physical measurements and before preparing the hexosomes. This will safeguard a good quality control measure in the preparation of the formulations.

4.1   Introduction

As mentioned in the Chapter 1, polar amphiphilic lipids that possess a low aqueous solubility in the presence of excess water often self-assemble into lyotropic liquid crystalline phases (Revathi & Dhanaraju, 2014). Self-assembly into lyotropic liquid crystalline phases is governed by local constraints that can be described in terms of the critical packing parameter (CPP). Critical packing parameter is defined as $v/\alpha_0 l_c$ where v is volume of the hydrophobic part of the surfactant molecule, α_0 is the effective head group surface area and l_c is the most extended chain length of surfactant tail. Furthermore, formation of inverse phases of double alkyl chain length glycolipids have been reported by numerous authors (Hato et al., 2002; Mannock et al., 2000; Zahid et al., 2013). Thus, the branched-chain glycolipid more likely to adopt inverse phase because when the molecule has a wedge-shape such that the polar head group is small in relation to the volume occupied by the hydrophobic chain where CPP>1 (calculation of CPP of inverse hexagonal showed in **Section 4.5.3**) (Hyde, 2001; Israelachvili et al., 1980a; Israelachvili et al., 1976b; Nagarajan, 2002; Revathi & Dhanaraju, 2014; Sagnella et al., 2009).

The dry compound of glycolipid ($\alpha\beta$-Glu-OC$_{10}$C$_6$) was assumed dried because it was difficult to eliminate all the water content in sugar lipids (Liew et al., 2015; Loewenstein & Igner, 1991). The water content of glycolipids was observed using Fourier transform infrared spectroscopy (FTIR) to evaluate its bending and stretching modes. The $\alpha\beta$-Glu-OC$_{10}$C$_6$ used was dried for at least 24 h. It was then left in ambient moisture for 96 h (room temperature) and in excess water for 72 h. FTIR spectra showed that the peak in the broad –OH stretching region between 3600 and 3200 cm^{-1} was smaller in the dry sample than in the samples at ambient moisture and in excess water. Furthermore, the water bending mode absorption at 1700-1600 cm^{-1} was almost insignificant in the dry sample, compared to those of the other two samples. The FTIR spectra of $\alpha\beta$-Glu-OC$_{10}$C$_6$ (three samples) are shown in the **Figure 4.1**
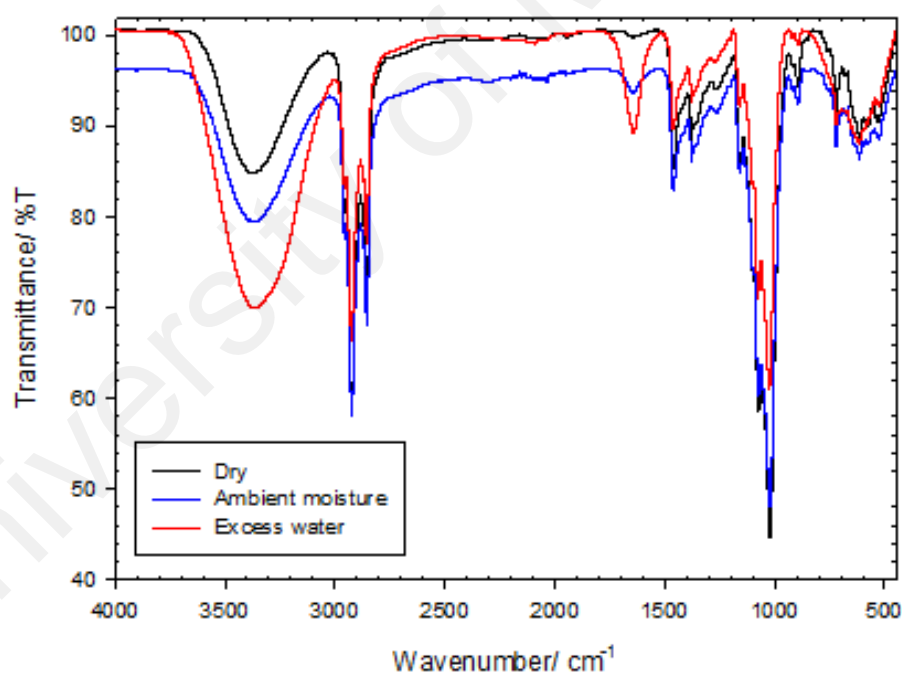
Figure 4.1: FTIR spectra for dried $\alpha\beta$-Glu-OC$_{10}$C$_6$ (freeze dried for at least 24 h), at ambient moisture for 96 h, and in excess water for 72 h.

4.2 Thermogravimetric Analysis

Thermogravimetric studies showed that $\alpha\beta$-Glu-OC$_{10}$C$_6$ started to decompose at 180°C upon heating as shown in **Figure 4.2**. Based on a previous study (Ahmad et al., 2012), the decomposition temperature of $\alpha\beta$-Glu-OC$_{10}$C$_6$ was at 175°C, which was a slightly smaller value. However, the obtained value was still comparable to that previously measured.
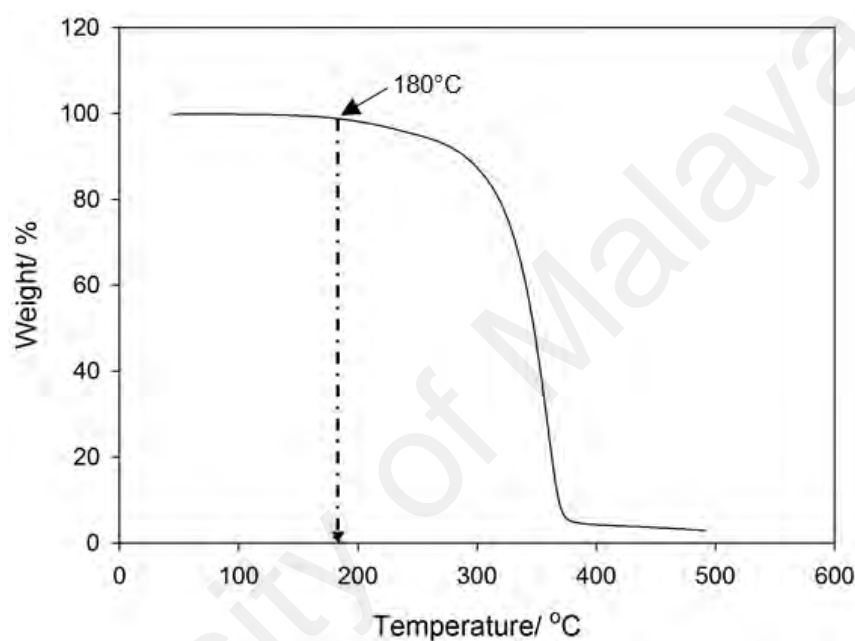
Figure 4.2: TGA thermogram of $\alpha\beta$-Glu-OC$_{10}$C$_6$.

4.3 Differential Scanning Calorimetry

The transition temperature of $\alpha\beta$-Glu-OC$_{10}$C$_6$ was obtained from the second heating cycle of peak, while the enthalpy change was calculated by transition peak obtained from graph software. $\alpha\beta$-Glu-OC$_{10}$C$_6$ showed a melting temperature of about 54°C (**Figure 4.3**) with enthalpy change, ΔH = -0.30 kJ mol^{-1}. No other phase transitions were observed upon heating and cooling. However, a previous study has reported that $\alpha\beta$-Glu-OC$_{10}$C$_6$ melting temperature was 57°C (Ahmad et al., 2012), which was slightly higher than currently measured, as a result of the purity of the samples being different (~90%). Moreover, the transition temperatures for the first heating and cooling were

slightly higher values than in the second heating and cooling cycle as shown in **Table 4.1**. However, the difference was negligible, and the reproducibility of DSC peaks indicated that the $\alpha\beta$-Glu-OC$_{10}$C$_6$ was stable towards thermal degradation (Ahmad et al., 2012).
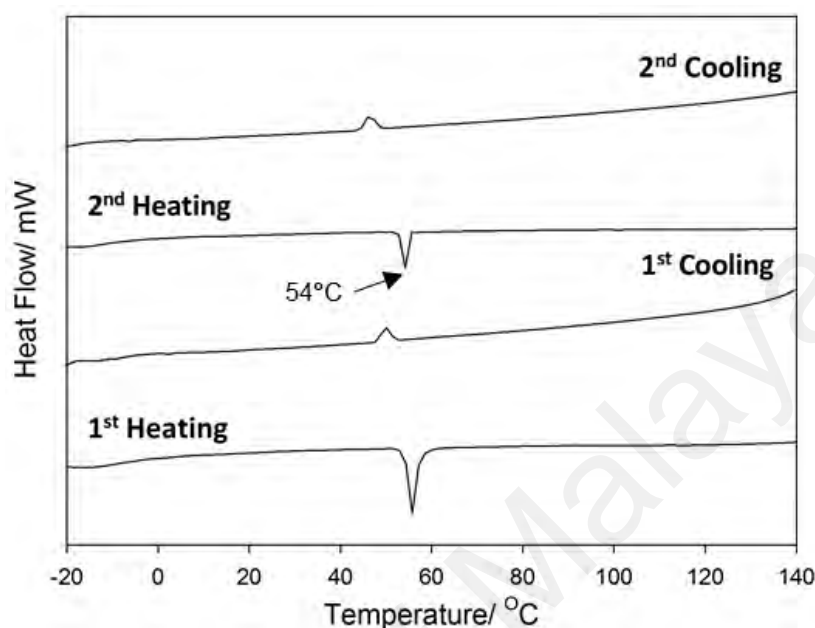
Figure 4.3: DSC thermogram of $\alpha\beta$-Glu-OC$_{10}$C$_6$ in two cycles of heating and cooling.

Table 4.1: The measured phase transition temperatures of $\alpha\beta$-Glu-OC$_{10}$C$_6$.

Molecular Formula $\alpha\beta$-Glu-OC$_{10}$C$_6$	Molecular Weight/ gmol^{-1}	Clearing Temperature / °C (First Cycle)		Clearing Temperature / °C (Second Cycle)		ΔH / kJ mol^{-1}
		Heating	Cooling	Heating	Cooling	
C$_{22}$H$_{44}$O$_6$	404.58	55.62	47.12	53.96	46.46	-0.30

4.4 Thermotropic and Lyotropic Phase Behaviour

At room temperature, $\alpha\beta$-Glu-OC$_{10}$C$_6$ existed physically as a yellowish gel-like syrup. By varying the temperature, the phase behaviour of dry $\alpha\beta$-Glu-OC$_{10}$C$_6$ surfactant was studied qualitatively using an optical polarizing microscope. The dried compound gave a strong birefringence with a defined texture under OPM. Upon heating at 5°C/min (**Figure 4.4a**), the sample melted from an ordered phase to an isotropic phase at around

57°C. Upon cooling into an anisotropic phase a focal conic texture of columnar phase was clearly observed as previously reported (Ahmad et al., 2012; Brooks et al., 2011; Zahid et al., 2013). A clearer focal conic texture appeared when a lower rate of cooling (1°C/min) was applied because $\alpha\beta$-Glu-OC$_{10}$C$_6$ molecules had more time to reorganize themselves (**Figure 4.4b**). The present anomeric mixture (90% β) of $\alpha\beta$-Glu-OC$_{10}$C$_6$, had a clearing temperature in between those of α and β anomers. Consistent with a previous study (Zahid et al., 2013), the pure α-Glu-OC$_{10}$C$_6$ became clear at 47.5°C from a lamellar phase ($L\alpha$), while pure β-Glu-OC$_{10}$C$_6$ in a columnar or hexagonal phase became isotropic at 76°C. The $\alpha\beta$-Glu-OC$_{10}$C$_6$ phase transition temperature was slightly different from that obtained by DSC (54±1°C), as expected, due to the sample experiencing a different decomposition rate in an aluminum pan from being on a glass plate (Laurent et al., 2003; Zahid et al., 2012).
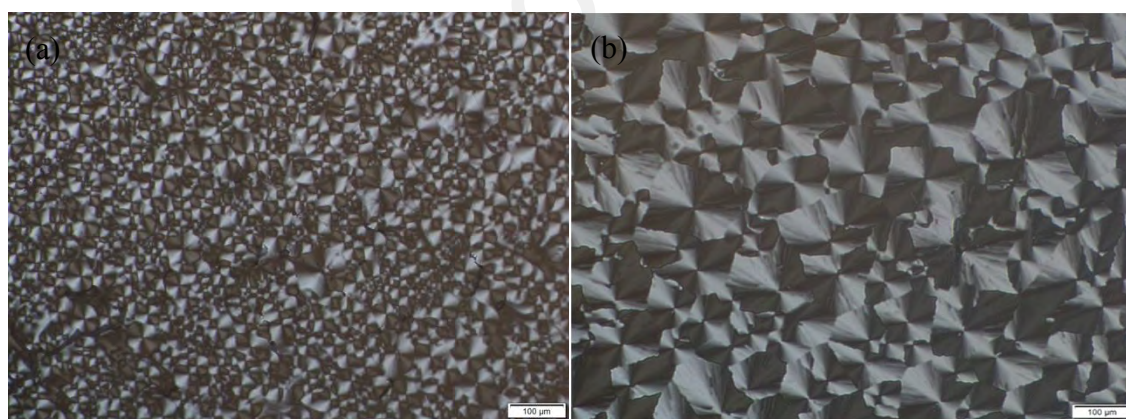
Figure 4.4: Optical polarizing micrographs of $\alpha\beta$-Glu-OC$_{10}$C$_6$ upon (a) heating and (b) cooling.

The lyotropic phase was determined via contact penetration experiment using OPM (Laughlin, 1992; Rendall et al., 1983; Sani et al., 2012). **Figure 4.5** shows the $\alpha\beta$-Glu-OC$_{10}$C$_6$ phase formation from higher to lower water content which corresponded to phase transition from an isotropic phase (*L*) to an inverse hexagonal phase (*H$_{II}$*) of $\alpha\beta$-Glu-OC$_{10}$C$_6$ at a constant temperature of 25°C. A previous study on pure β-Glu-OC$_{10}$C$_6$ and technical grade $\alpha\beta$-Glu-OC$_{10}$C$_6$ has shown the formation of an inverse hexagonal phase (Ahmad et al., 2012; Zahid et al., 2013).
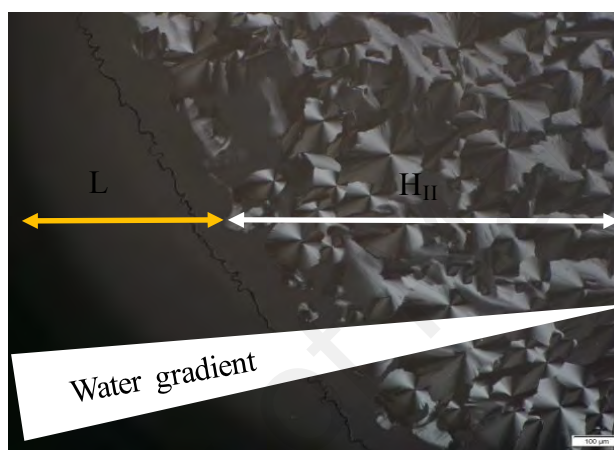
Figure 4.5: Optical polarised micrograph of the contact penetration experiment for $\alpha\beta$-Glu-OC$_{10}$C$_6$ at 25°C.

4.5 Phase Structure from Small-Angle X-ray Scattering (SAXS)

4.5.1 Dry $\alpha\beta$-Glu-OC$_{10}$C$_6$

Figure 4.6a shows the scattering patterns of a dry $\alpha\beta$-Glu-OC$_{10}$C$_6$ at different temperatures from 25°C to 100°C. At temperatures below 60°C, the pattern consisted of three peaks with spacing ratios of $\sqrt{1}$, $\sqrt{3}$ and $\sqrt{4}$, where the latter two peaks were weaker than the first one. This scattering pattern was a typical assignment for hexagonal phase as reported previously by Seddon (Brooks et al., 2011; Seddon, 1990). This assignment has been confirmed by those of OPM at the same temperatures. This result was slightly different from that found by Zahid *et al.* (Zahid et al., 2013) for pure β-Glu-OC$_{10}$C$_6$ (**Figure 4.6b**), which gave only one peak for a dry hexagonal phase at $\sqrt{1}$. In

their case, the second peak at $\sqrt{3}$ was suppressed because the form factor of a single (dry) cylinder (a Bessel function) has its first node beyond the first reflection. On the other hand, the higher order lobes were characteristically of low amplitude for dry cylinder. Therefore, they observed only the first reflection (Liew et al., 2015; Zahid et al., 2013). A similar result was observed for dry inverse hexagonal phase, H_{II} of phospholipids where the higher-order peaks $\sqrt{3}$, $\sqrt{4}$, $\sqrt{7}$ etc. of 2-D hexagonal structure were not observed due to the form factor effect (Brooks et al., 2011; Liew et al., 2015; Zahid et al., 2013). Therefore, it was interesting to observe that technical grade $\alpha\beta$-Glu-OC$_{10}$C$_6$, which consisted of 10% α anomer, gave 3 peaks instead of only one, as observed before for pure grade β-Glu-OC$_{10}$C$_6$. In addition, an inverse hexagonal phase was more favoured for dry $\alpha\beta$-Glu-OC$_{10}$C$_6$ because of the weak hydrogen bond interactions in the sugar headgroup region which promoted the assembly to adopt an inverse curvature, allowing the chain to splay (Seddon et al., 2000).

For dry $\alpha\beta$-Glu-OC$_{10}$C$_6$, the lattice parameter of the inverse hexagonal phase became smaller with increasing temperature. These results and the corresponding lattice parameters are summarised in **Table 4.2**. At 60°C and above (**Figure 4.6a**), a broad peak was observed signifying the system had melted to an optically isotropic phase which was expected to be inverse micellar phase L_2, since water was absent (Brooks et al., 2011). **Table 4.2** also gave the lattice parameters for pure α-Glu-OC$_{10}$C$_6$ and pure β-Glu-OC$_{10}$C$_6$ at different temperatures from a previous study (Zahid et al., 2013). The β dominant lipid favoured H_{II}, while α compounds favoured lamellar, $L\alpha$.

Table 4.2: Lattice parameter of dried and hydrated $\alpha\beta$-Glu-OC$_{10}$C$_6$ obtained from SAXS experiment and in comparison with the pure compounds (Zahid et al., 2013).

$\alpha\beta$-Glu-OC$_{10}$C$_6$	Lattice parameter, a/nm	
	Dried	Hydrated
Temperature/°C		
25	2.918 (H_{II})	4.176 (H_{II})
40	2.914 (H_{II})	4.206 (H_{II})
60	2.895 (H_{II})	4.078 (H_{II})
80	2.885 (L_{II})	3.198 (L_I)
100	2.877 (L_{II})	3.122 (L_I)
Pure α-Glu-OC$_{10}$C$_6$ (Zahid et al., 2013)		
24	2.390 ($L\alpha$)	5.920 ($Pn3m$)
37	2.440 ($L\alpha$)	5.830 ($Pn3m$)
62	NA	5.880 ($Pn3m$)
Pure β-Glu-OC$_{10}$C$_6$ (Zahid et al., 2013)		
24	2.870 (H_{II})	8.720 ($Ia3d$), 5.580 ($Pn3m$)
37	2.910 (H_{II})	8.750 ($Ia3d$)
62	2.850 (H_{II})	r.d. ($Ia3d$), r.d. ($Pn3m$)

The lattice parameter for pure hydrated α-Glu-OC$_{10}$C$_6$ obtained at 80.0% (w/w) and β-Glu-OC$_{10}$C$_6$ obtained at 80.3% (w/w)
Error in lattice parameter measurement is < 0.01nm
r.d. denotes radiation damaged; NA denotes not available
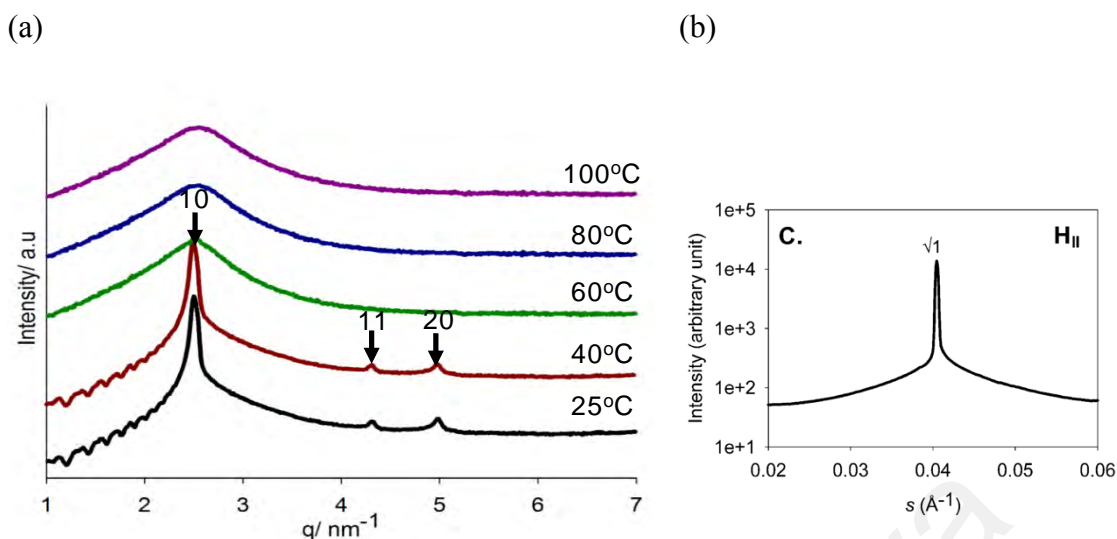
Figure 4.6: SAXS patterns of (a) a dry technical grade $\alpha\beta$-Glu-OC$_{10}$C$_6$ at different temperatures (b) pure β-Glu-OC$_{10}$C$_6$. Adopted from (Zahid et al., 2013).

4.5.2 Hydrated $\alpha\beta$-Glu-OC$_{10}$C$_6$

Branched-chain glycolipid $\alpha\beta$-Glu-OC$_{10}$C$_6$ in excess water was investigated at temperatures from 25°C to 100°C, as shown in **Figure 4.7**. At temperatures lower than 80°C, the SAXS pattern for $\alpha\beta$-Glu-OC$_{10}$C$_6$ was consistent with that of inverse hexagonal phase, H_{II} phase with strong characteristic peaks of $\sqrt{1}$, $\sqrt{3}$ and $\sqrt{4}$. This scattering pattern has confirmed H_{II} phase as compared with OPM results. The H_{II} phase are frequently stable in the presence of excess water and the bilayer chains point outward from cylinder surface or bend toward water region known as pivotal plane (negative curvature), while the polar headgroups filled with aqueous solution (Perutková et al., 2009a; Perutková et al., 2011b). This finding was in contrast to a previous study for pure β-Glu-OC$_{10}$C$_6$ in excess water, at a similar range of temperatures (see **Table 4.2**), that gave an inverse bicontinuous cubic (Zahid et al., 2013). As expected, because of the hydration effect (Ahmad et al., 2012), the lattice parameters for hydrated $\alpha\beta$-Glu-OC$_{10}$C$_6$ were larger and the peaks are more intense than in the case of dried $\alpha\beta$-Glu-OC$_{10}$C$_6$ (**Table 4.2**). At higher temperatures (80°C and 100°C), broad peaks were observed indicating an isotropic phase, as expected, rather than the normal micellar phase L_I in the

presence of water. The presence of an inverse hexagonal phase, H_{II} could be assumed from the hydrophobic effect (Rappolt et al., 2003). This effect resulting H_{II} phase, where lipids can adopt negative curvature (inverse) at interface, allowing the chains to splay (Rappolt, 2006). Besides, the volume occupied by the branched-chain hydrophobic part was bigger than the volume of the hydrophilic part of a single glucose unit. Thus, H_{II} phase was formed (Hyde, 2001), as supported by the critical packing parameter (CPP) for $\alpha\beta$-Glu-OC$_{10}$C$_6$ calculated as 1.40 (Ahmad et al., 2012). From this structural study, we conclude that the technical grade of β dominant $\alpha\beta$-Glu-OC$_{10}$C$_6$ in excess water gave a hexagonal assembly, while the pure β-Glu-OC$_{10}$C$_6$ grade stabilized the cubic phases.
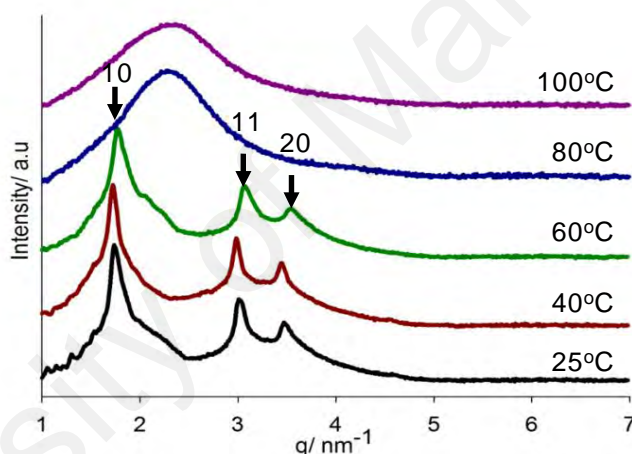
Figure 4.7: SAXS patterns of hydrated technical grade $\alpha\beta$-Glu-OC$_{10}$C$_6$ at different temperatures.

4.5.3 Calculation Critical Packing Parameter (CPP)

The critical packing parameter (CPP) was defined as (Israelachvili et al., 1980a; Israelachvili et al., 1976b)

$$CPP = \frac{v}{a_o lc} \tag{4.1}$$

where v was the volume of the hydrophobic part of the surfactant molecule, a_o was the effective headgroup surface area and l_c the most extended chain length of surfactant tail. v was determined from the density and molecular weight of the hydrophobic part, and l_c was calculated by using Tanford equation (Tanford, 1972), assuming that the length of the hydrophobic part was equal to the length of the longest alkyl chain. In the case of a branched $C_{10}C_6$ alkyl chain, 0.99 nm and 0.45 nm^3 were calculated for l_c and v, respectively.

The a_o surface was independently calculated for the two mesostructures studied by SAXS experiment (inversed hexagonal). The calculation method and their results were described as:

Inversed hexagonal phase ($\alpha\beta$-Glu-OC$_{10}$C$_6$)

In hexagonal phase, the area per molecule at the hydrophilic-lipophilic boundary, $a_o = 0.325$ nm^2 was determined by **Equation 4.2** (Sharma et al., 2006)

$$a_o = \frac{2vH}{rH} \tag{4.2}$$

where vH and rH were the volume and the length respectively of the hydrophilic parts of the molecule. rH was also calculated from the d-spacing determined by SAXS as shown in **Equation 4.3**. Thus,

$$rH = d\sqrt{\frac{2\emptyset H}{\sqrt{3}\,\pi}} \tag{4.3}$$

where $\emptyset_H$ was the volume fraction of the hydrophilic part of the molecule, which was calculated from **Equation 4.4**:

$$\emptyset H = \frac{vH}{vS}\emptyset S \tag{4.4}$$

In the case of $\alpha\beta$-Glu-OC$_{10}$C$_6$ (nonionic surfactant), the experimental d-spacing, $a = 2d/\sqrt{3}$ was 3.617 nm, the volumes of the surfactant molecule, $vS = 0.67$ nm^3 and the polar head, $vH = 0.19$ nm^3, were calculated from mass and density, and $\emptyset s$ was assumed to be 1.

Therefore, the value of the critical packing parameter (CPP) **Equation 4.1** was 1.40, obtained from the branched-chain glycolipid surfactant. The definition of the critical packing parameter implied that larger than 1 would result in an inversed phase, which was significant in our experiment.

4.6   Critical Aggregation Concentration (CAC)

The presence of molecular aggregates could be assumed when the surfactant solution changed from a clear to a turbid solution at a very low concentration, called the critical aggregation concentration (CAC). **Figure 4.8** gives the plot of the surface tension of $\alpha\beta$-Glu-OC$_{10}$C$_6$ solutions (in the technical grade and in the mixture with co-surfactants of 10:1 of $\alpha\beta$-Glu-OC$_{10}$C$_6$:Tween series) as a function of the log concentration. On increasing the concentration, the surface tension was reduced to a minimum value of 0.0070 mM, which also marked the CAC for $\alpha\beta$-Glu-OC$_{10}$C$_6$ (Ahmad et al., 2012). The critical aggregation concentration (CAC) of all systems are summarised in **Table 4.3**.
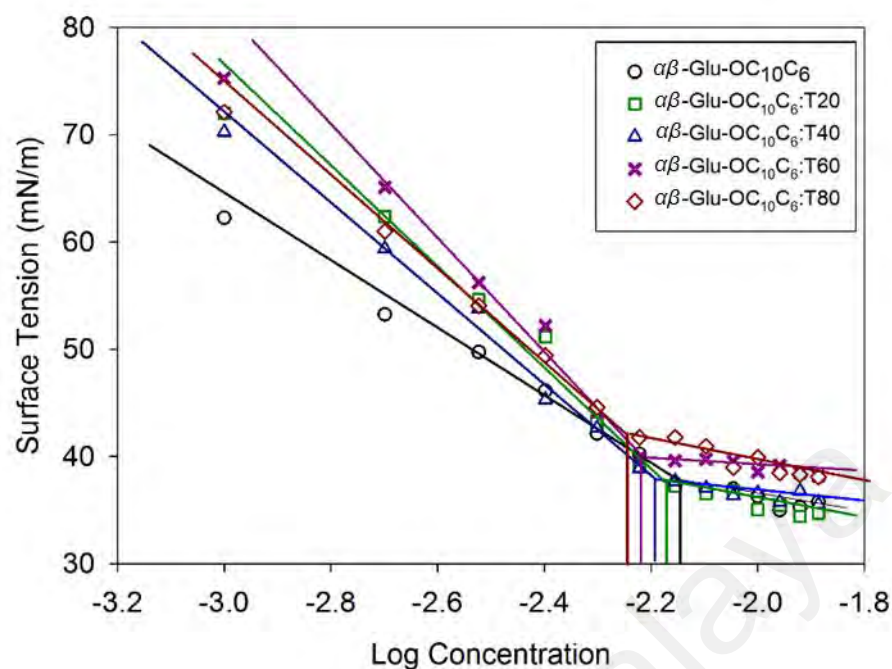
Figure 4.8: Surface tension profiles of $\alpha\beta$-Glu-OC$_{10}$C$_6$ and mixture of 10:1 of $\alpha\beta$-Glu-OC$_{10}$C$_6$:Tween series as a function of log concentration at 25°C.

The aggregation behaviours of addition Tween series into the nonionic surfactant of $\alpha\beta$-Glu-OC$_{10}$C$_6$ reduced the CAC value of $\alpha\beta$-Glu-OC$_{10}$C$_6$ (see **Table 4.3)**, in the order of $\alpha\beta$-Glu-OC$_{10}$C$_6$ > $\alpha\beta$-Glu-OC$_{10}$C$_6$:T20 > $\alpha\beta$-Glu-OC$_{10}$C$_6$:T40 > $\alpha\beta$-Glu-OC$_{10}$C$_6$:T60 > $\alpha\beta$-Glu-OC$_{10}$C$_6$:T80. Tween series had an equal number of hydrophilic PEG units and the major difference lay in the number of hydrophobic tails of methylene group, which decreased in the order of T80 (C$_{18}$) = T60 (C$_{18}$) > T40(C$_{14}$) > T20(C$_{12}$). Surfactants with long hydrophobic tails with PEG moieties were more stable at the surface of $\alpha\beta$-Glu-OC$_{10}$C$_6$ than were those with short tails (Sekhar et al., 2019; Zhao et al., 2010). Compared to T60, T80 had the lowest CAC value even though they had the same alkyl chain length (Garofalakis et al., 2000). This might have resulted from the double bond in the alkyl chain of T80, which did not exist in other Tween series. Thus, the double bond strengthened the adsorption of T80 on $\alpha\beta$-Glu-OC$_{10}$C$_6$ through the interaction of the π orbital of the double bond (Kothekar et al., 2007; Zhao et al., 2010). This result was typical of that found for nonionic-nonionic surfactants mixture. Even though such mixture

58

comprised of weak molecular interaction, a higher mutual solubility was observed (Huibers & Shah, 1997). Two factors contributed to this phenomenon, namely geometrical packing of the headgroup and the length of the hydrophobic tails (Boyd et al.,1972; Posocco et al., 2016).

Table 4.3: CAC values of $\alpha\beta$-Glu-OC$_{10}$C$_6$ and mixture of 10:1 of $\alpha\beta$-Glu-OC$_{10}$C$_6$:Tween series (T20, T40, T60 and T80) solutions.

Surfactant solution	CAC (mM)
$\alpha\beta$-Glu-OC$_{10}$C$_6$	0.0070
$\alpha\beta$-Glu-OC$_{10}$C$_6$:T20	0.0065
$\alpha\beta$-Glu-OC$_{10}$C$_6$:T40	0.0062
$\alpha\beta$-Glu-OC$_{10}$C$_6$:T60	0.0059
$\alpha\beta$-Glu-OC$_{10}$C$_6$:T80	0.0056

Uncertainty in the measurement was less than 5%

4.7 Hexosome Formation by $\alpha\beta$-Glu-OC$_{10}$C$_6$

Like before, water dispersed $\alpha\beta$-Glu-OC$_{10}$C$_6$ led to hexosomes formation derived from an inverse hexagonal phase, H_{II}. Here, the formation of an inverse hexagonal liquid crystalline nanoparticles (hexosomes) using $\alpha\beta$-Glu-OC$_{10}$C$_6$ was investigated based on the top-down approach (Chen et al., 2014; Guo et al., 2010). From the particle sizer measurement, the average hydrodynamic size (Z-average) and polydispersity index (PDI) of the prepared hexosomes are reported in **Table 4.4**. The mean particle size of $\alpha\beta$-Glu-OC$_{10}$C$_6$ was similar to those reported in the literature for glycerolmonooleate (GMO), with a size range of 100-500 nm (Amar-Yuli et al., 2007; Gustafsson et al.,1997). **Figure 4.9a** shows the TEM micrographs of $\alpha\beta$-Glu-OC$_{10}$C$_6$ hexosomes that were observed as hexagonal or spherically shaped particles of about 50-120 nm in diameter. The $\alpha\beta$-Glu-OC$_{10}$C$_6$ dispersion in water was unstable and the particle has started to

precipitate after 5 days onwards. The reason for the low dispersion stability was the relatively high PDI which significantly influenced the dispersion stability (**Table 4.4**). The higher PDI leads to bigger average hydrodynamic size of $\alpha\beta$-Glu-OC$_{10}$C$_6$ dispersion suggesting that there would be little or more flocculation or coalescence occurred (Loi et al., 2019; Ryu et al., 2018).

Table 4.4: Average hydrodynamic size (Z-average) and polydispersity index (PDI) of the dispersed nanoparticles of $\alpha\beta$-Glu-OC$_{10}$C$_6$ and mixture of 10:1 of $\alpha\beta$-Glu-OC$_{10}$C$_6$:Tween series solutions.

Surfactant solution	Z-average (nm)	PDI
$\alpha\beta$-Glu-OC$_{10}$C$_6$	145 ± 3	0.251
$\alpha\beta$-Glu-OC$_{10}$C$_6$:T20	106 ± 3	0.248
$\alpha\beta$-Glu-OC$_{10}$C$_6$:T40	96 ± 2	0.160
$\alpha\beta$-Glu-OC$_{10}$C$_6$:T60	89 ± 2	0.165
$\alpha\beta$-Glu-OC$_{10}$C$_6$:T80	85 ± 1	0.165

Hexosomes from nonionic surfactant such as $\alpha\beta$-Glu-OC$_{10}$C$_6$ was unstable, since the hydrophilic-lipophilic balance (HLB) of the surfactant was not optimum to allow the formation of a stable double layer as previously reported (Ahmad et al., 2012; Hato, 2001). Therefore, to enhance the stability of $\alpha\beta$-Glu-OC$_{10}$C$_6$ hexosomes, an investigation of $\alpha\beta$-Glu-OC$_{10}$C$_6$:Tween series surfactant mixtures was performed. Standard nonionic surfactant (Tween series) was chosen for this purpose. An optimised ratio of 10:1 of $\alpha\beta$-Glu-OC$_{10}$C$_6$ to Tween series was selected after several different formulation ratios were tested.
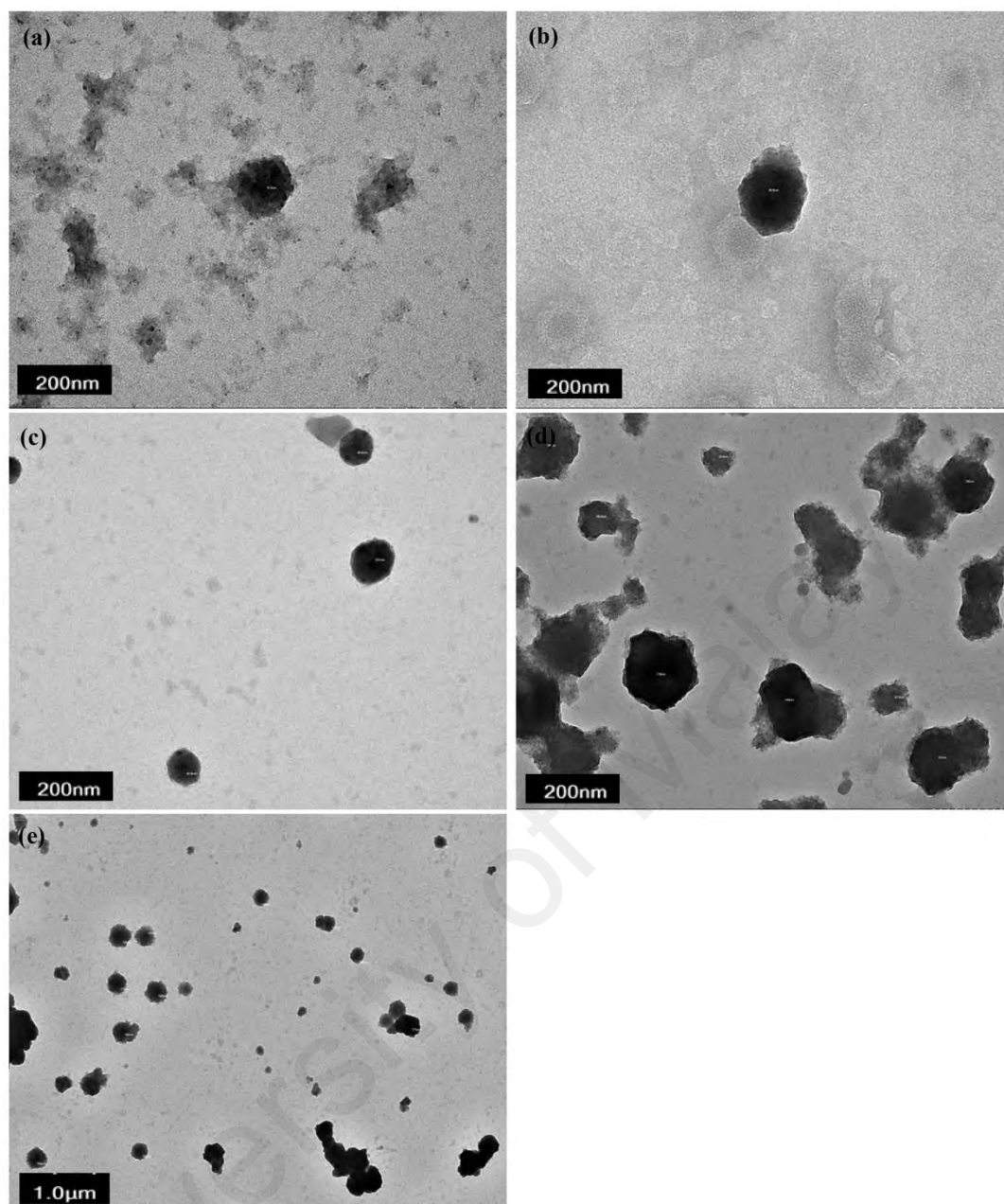
Figure 4.9: TEM micrographs of the dispersed particles of inverse hexagonal phase in water (hexosomes) of (a) branched-chain glucoside; $\alpha\beta$-Glu-OC$_{10}$C$_6$ (b) mixture of $\alpha\beta$-Glu-OC$_{10}$C$_6$:T20 (c) mixture of $\alpha\beta$-Glu-OC$_{10}$C$_6$:T40 (d) mixture of $\alpha\beta$-Glu-OC$_{10}$C$_6$:T60 and (e) mixture of $\alpha\beta$-Glu-OC$_{10}$C$_6$:T80.

The composition of mixture affected the particle size and PDI of the dispersion when stabilising agent were used in the formulation (González-Reza et al., 2018). From the measurement of particle sizer, the addition of co-surfactant (Tween series) reduced the average hydrodynamic size and also the PDI of the mixtures, as shown in **Table 4.4**. The ratio mixture of 10:1 of $\alpha\beta$-Glu-OC$_{10}$C$_6$:T80 hexosomes exhibited smaller particles size and PDI than those in the other Tween series. The mixtures of $\alpha\beta$-Glu-

OC$_{10}$C$_6$:Tween series hexosomes were also visualised by TEM (**Figure 4.9b-e**), and indicated that hexagonal or spherically shaped particles were formed with size ranging between 30 and 90 nm in diameter. The hexosome particle's size determined by TEM did not correspond to the average hydrodynamic size measured by a particle sizer because the latter was determined through an indirect method of dynamic light scattering. The hydrodynamic size from the scattering of particles was usually bigger than that by TEM that was observed directly from an electron microscope, and this gave the actual size of hexosomes (Domingos et al., 2009; Filella et al.,1997; Fissan et al., 2014).

4.8 Stability Study of Hexosomes

4.8.1 Light Backscattering

The backscattered light profiles of glycolipid over the total height of samples are shown in **Figure 4.10**, in which the measurements were taken for more than 24 h. In general, backscattered light was different at the top and bottom of the samples as a result of different concentrations of dispersed particles. Therefore, the measured backscattered (BS) was inversely proportional to square root $\lambda*$ as given in the following **Equation 4.5** (Azema, 2006; Celia et al., 2009; Mengual et al., 1999),

$$BS \approx 1/\sqrt{\lambda*} \tag{4.5}$$

From Mie theory in **Equation 4.6** [49-51], $\lambda*$ (µm) the photon transport length was proportional to particle diameter, d (µm) particle diameter and inversely proportional to the volume fraction, and ϕ (%) volume fraction of the particles. Thus,

$$\lambda*(d,\phi) = 2d/[3\phi(1-g)Qs], \tag{4.6}$$

where g and Qs were optical parameters.

As mentioned previously, the $\alpha\beta$-Glu-OC$_{10}$C$_6$ dispersion in water was unstable as shown in backscattered profile (**Figure 4.10**). A technical grade branched-chain glycolipid and the mixed branched-chain glycolipid-Tween series samples displayed similar patterns with regard to their backscattered profiles (**Figure 4.10a-e**), where the light signals at the top part of the backscattered profile (50-55 mm) decreased with time. However, the light signals at the bottom part of the backscattered profile (5-10 mm) increased with time except for **Figure 4.10a** (signal was indistinct) and **Figure 4.10c** (packing in the sediment). This observation could be explained in terms of **Equations 4.5** and **Equation 4.6**, whereby BS decreased when ϕ decreased, which caused a decrease in the concentration of the samples within the top part, known as sedimentation (Buron et al., 2004; Mengual et al., 1999).

(a) $\alpha\beta$-Glu-OC$_{10}$C$_6$

(b) $\alpha\beta$-Glu-OC$_{10}$C$_6$:T20

(c) $\alpha\beta$-Glu-OC$_{10}$C$_6$:T40
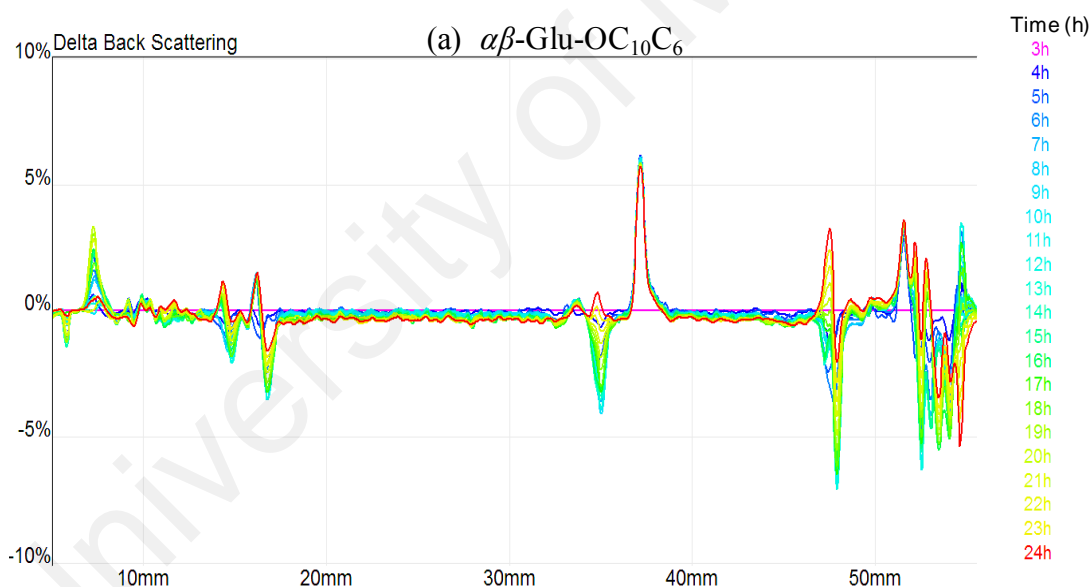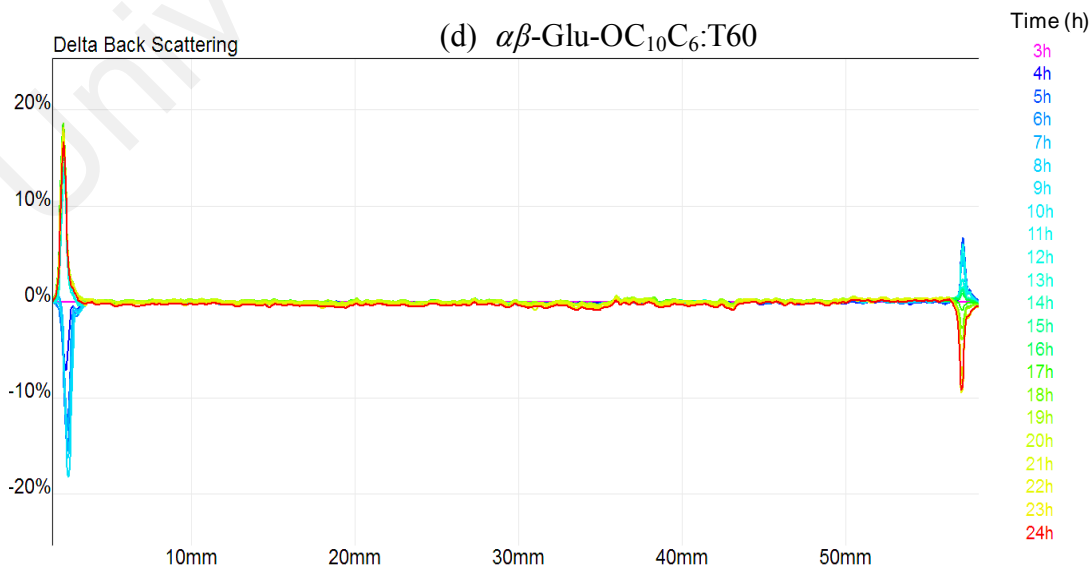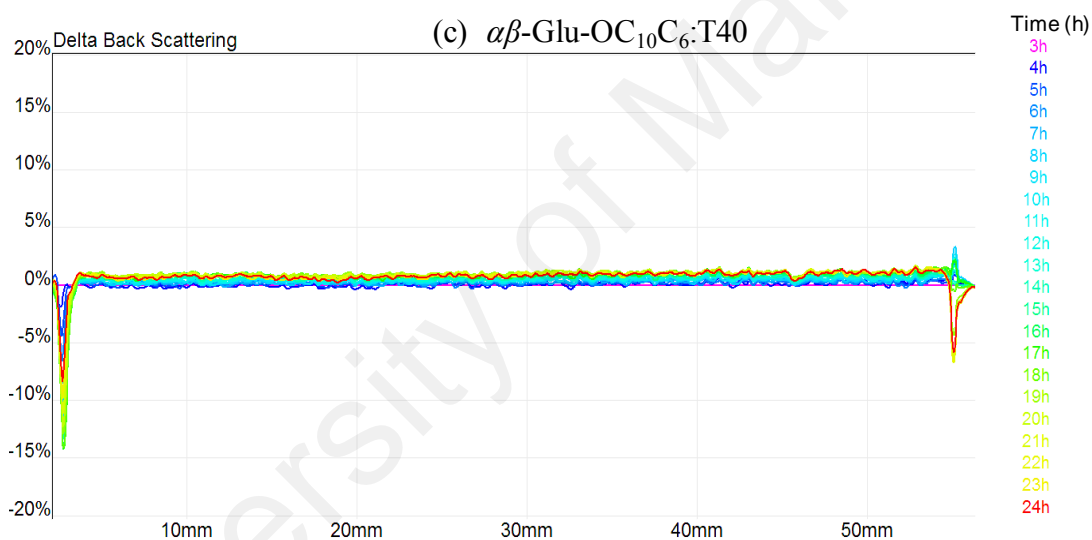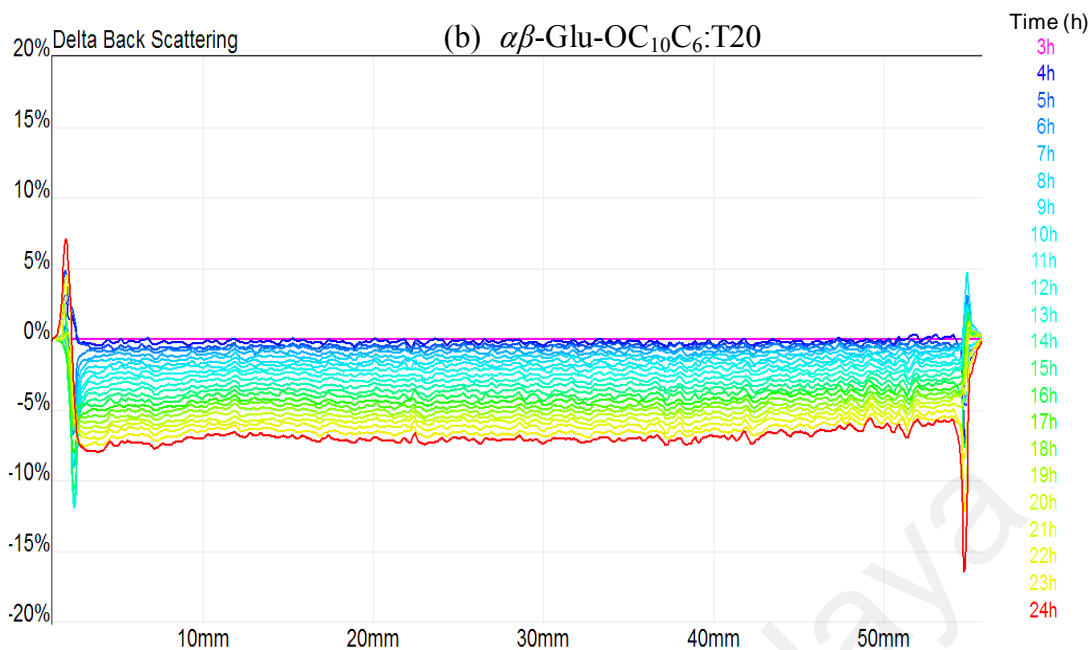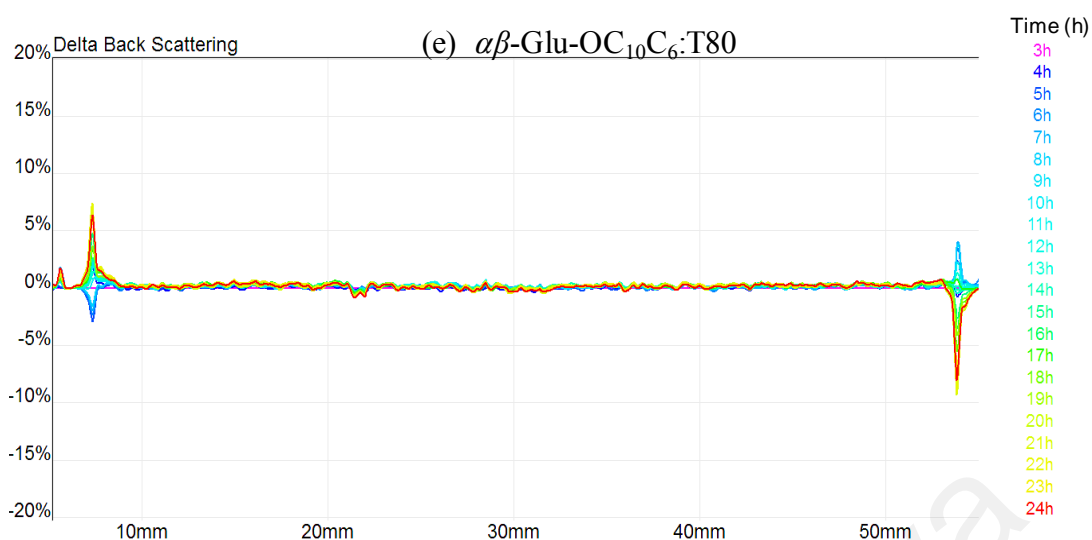
(d) $\alpha\beta$-Glu-OC$_{10}$C$_6$:T60

Figure 4.10: Backscattered light profiles of (a) $\alpha\beta$-Glu-OC$_{10}$C$_6$ (b) mixture of $\alpha\beta$-Glu-OC$_{10}$C$_6$:T20 (c) mixture of $\alpha\beta$-Glu-OC$_{10}$C$_6$:T40 (d) mixture of $\alpha\beta$-Glu-OC$_{10}$C$_6$:T60 and (e) mixture of $\alpha\beta$-Glu-OC$_{10}$C$_6$:T80 hexosomes samples.

The peak thickness kinetics (absolute thickness) against time was computed in order to investigate particle migration based on the top part of the sample's profile (50-55 mm), as shown in **Figure 4.11**. Generally, a high gradient of the graph implies the rate of sedimentation of the particles in the suspension increase (Ali et al., 2019; Tan et al., 2015; Yin et al., 2019). The deduction is the gradient of the samples $\alpha\beta$-Glu-OC$_{10}$C$_6$:T40, $\alpha\beta$-Glu-OC$_{10}$C$_6$:T60 and $\alpha\beta$-Glu-OC$_{10}$C$_6$:T80 were not steep as the sedimentation particles occurred because the y-axis values of these samples were small. The small sedimentation could be neglected which indicated that these samples ($\alpha\beta$-Glu-OC$_{10}$C$_6$:T40, $\alpha\beta$-Glu-OC$_{10}$C$_6$:T60 and $\alpha\beta$-Glu-OC$_{10}$C$_6$:T80) were stable. The branched-chain glycolipid was stabilised and sedimentation prevented due to the Tween series, especially T80. In the formation of the self-assembly structure, compared to the other Tween series, the latter was more miscible, able to penetrate better, swelled the liquid crystalline phase and promoted dispersion formation (Barauskas et al., 2006; Chen et al., 2016; Soliman et al., 2017). However, $\alpha\beta$-Glu-OC$_{10}$C$_6$ and $\alpha\beta$-Glu-OC$_{10}$C$_6$:T20 samples

had the highest gradient after 4 h and 9 h respectively, which indicated the rate of sedimentation of these samples were the highest.
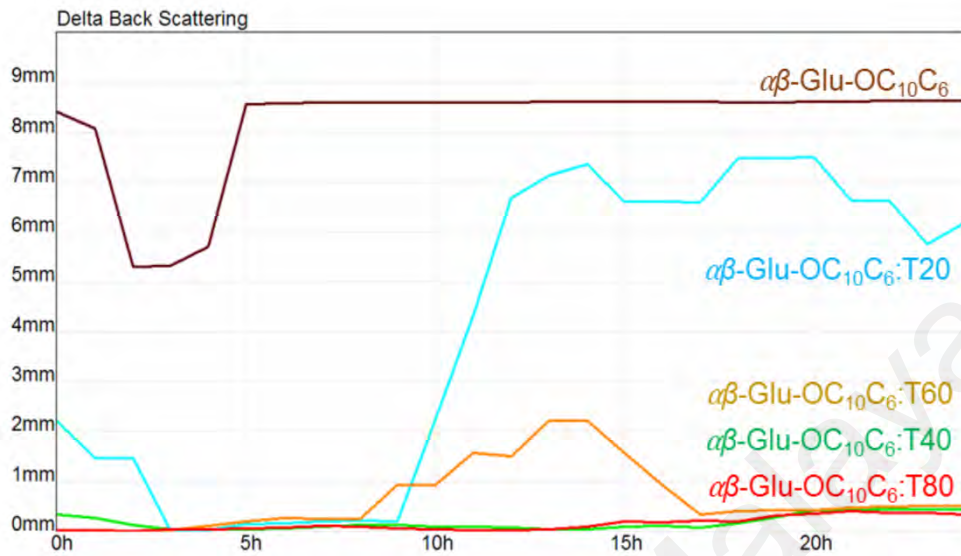
Figure 4.11: Peak thickness kinetics of $\alpha\beta$-Glu-OC$_{10}$C$_6$ and $\alpha\beta$-Glu-OC$_{10}$C$_6$:Tween series hexosomes at the top segment for all samples.

The middle portion of each profile (10-50 mm) was almost flat, which indicated that particle size of the samples remained unchanged except for $\alpha\beta$-Glu-OC$_{10}$C$_6$ and $\alpha\beta$-Glu-OC$_{10}$C$_6$:T20, as shown in **Figure 4.12**. Compared to that of $\alpha\beta$-Glu-OC$_{10}$C$_6$, the mean value kinetics over total height for $\alpha\beta$-Glu-OC$_{10}$C$_6$:T20 sample declined abruptly, which implied that the particle size of this sample increased over time. In this case, the decrement in the mean value kinetics indicated an increase in particle size, which was probably due to the agglomeration of the particles (Tan et al., 2015). However, the particles in $\alpha\beta$-Glu-OC$_{10}$C$_6$ and $\alpha\beta$-Glu-OC$_{10}$C$_6$:T20 samples were well dispersed in deionised water.
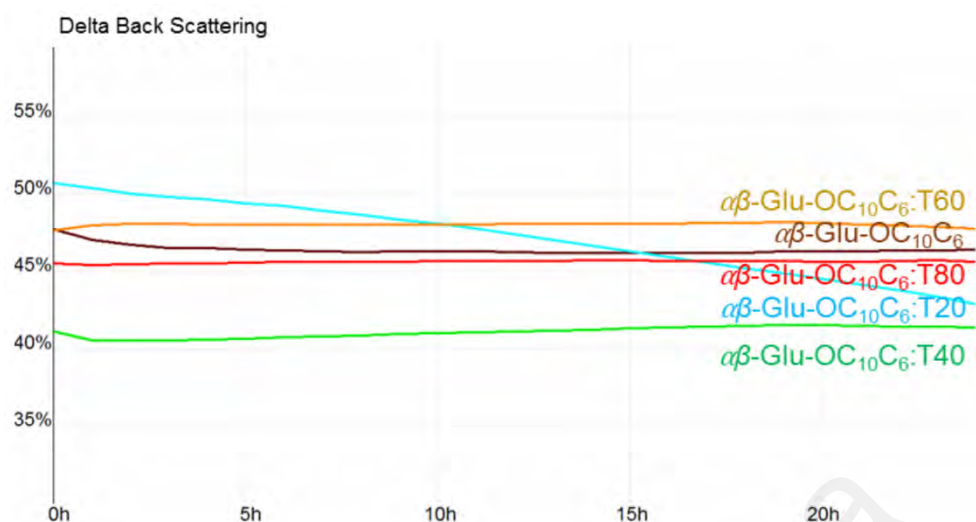
Figure 4.12: Mean value kinetics of $\alpha\beta$-Glu-OC$_{10}$C$_6$ and $\alpha\beta$-Glu-OC$_{10}$C$_6$:Tween series hexosomes at the middle segment for all samples.

4.8.2 Dynamic Light Scattering

The stability of $\alpha\beta$-Glu-OC$_{10}$C$_6$ hexosomes was found to improve when Tween series was added. **Figure 4.13** shows the $\alpha\beta$-Glu-OC$_{10}$C$_6$ and mixture of 10:1 of $\alpha\beta$-Glu-OC$_{10}$C$_6$:Tween series samples. The $\alpha\beta$-Glu-OC$_{10}$C$_6$ dispersion in water was unstable as it started to precipitate after 5 days and resulted in a rapid increase in average hydrodynamic size at 25ºC and 40ºC. The addition of Tween series to $\alpha\beta$-Glu-OC$_{10}$C$_6$ was able to reduce the average hydrodynamic size of the hexosomes. Among the Tween series, the mixture of $\alpha\beta$-Glu-OC$_{10}$C$_6$:T20 was unstable as it started to precipitate after 3 days. This result confirmed the former finding (see **Figure 4.12**) where the mixture $\alpha\beta$-Glu-OC$_{10}$C$_6$:T20 also declined rapidly. This result was typical of that of short alkyl chains, which formed more unstable dispersion than the long chains (Zhao et al., 2010). However, the mixture of $\alpha\beta$-Glu-OC$_{10}$C$_6$:T40 started to precipitate after 2 weeks at temperatures of 25ºC and 40ºC. It can be found that the particle size had a small increase at different temperature of 25ºC and 40ºC with the extension of the storage time (1 months). In this cases, the higher the temperature, the smaller the particle size diameter which contradict to Chai et al., Ryu et al., and Gonzalez-Reza et al. as for them increase

in particle size with increasing the temperature due to effect either Ostwald ripening and/or coalescence (Chai et al., 2019; González-Reza et al., 2018; Ryu et al., 2018). Additionally, the mixture of $\alpha\beta$-Glu-OC$_{10}$C$_6$:T60 and $\alpha\beta$-Glu-OC$_{10}$C$_6$:T80 was stable since they did not precipitate after 2 weeks and there was only a small increment in the average hydrodynamic size throughout the 4 weeks. After 6 weeks, the mixture of $\alpha\beta$-Glu-OC$_{10}$C$_6$:T80 was the most stable dispersed in aqueous solution. Thus, the mixture of $\alpha\beta$-Glu-OC$_{10}$C$_6$:T80 could be used as an alternative drug carrier system in the future.
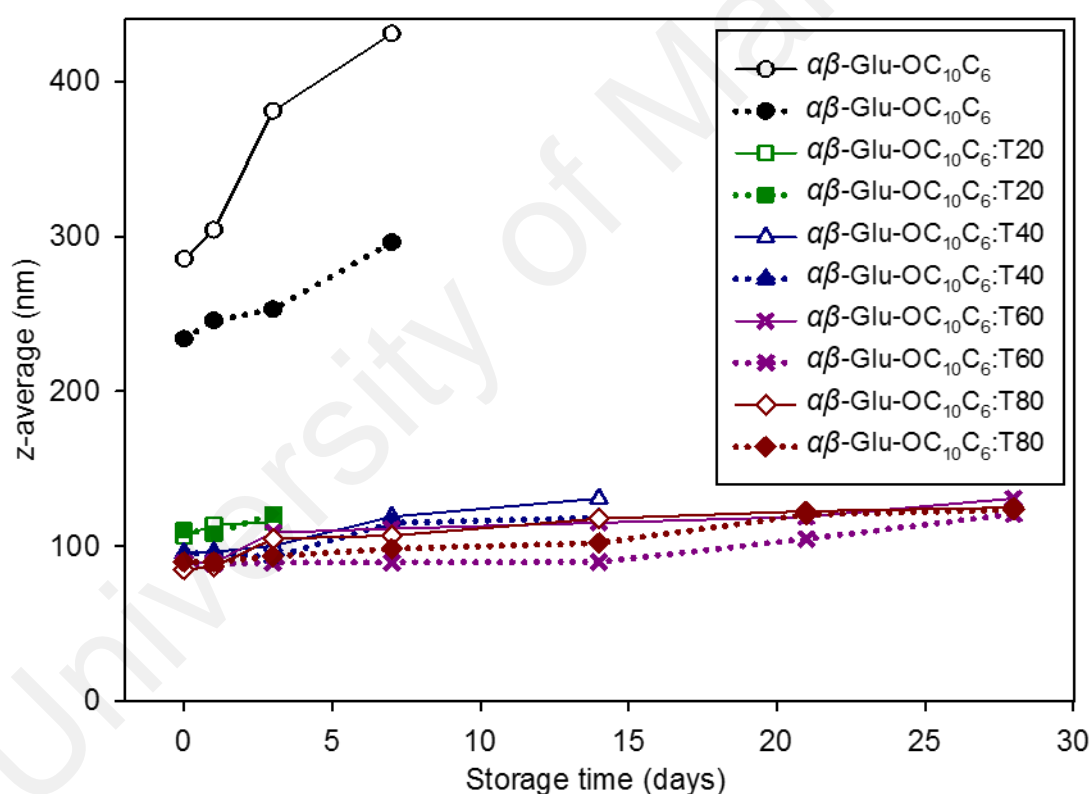
Figure 4.13: Effect of Tween series on the average hydrodynamic diameter of $\alpha\beta$-Glu-OC$_{10}$C$_6$ hexosomes, and their storage stability for 1 month.
Line representation: ——— 25°C; ·········· 40°C

The use of the Tween series as nanoparticle stabiliser have been reported extensively (Barauskas et al., 2006; Chen et al., 2016; Jiang et al., 2017; Shah et al., 2016; Soliman et al., 2017; Zhao et al., 2010) as shown in **Table 4.5**. The reason for this is thought to be due to the presence of PEG which increases the hydrophilicity of the surface (Chen et al., 2016). With the exception of the surface coating application of PTFE-water interface, where the addition of T80 led to a lower stability (Shah et al., 2016), generally T80 improves the stability of the nanoparticles better compared with the other Tween series members. Additionally, it leads a smaller particle size and size distribution (Barauskas et al., 2006; Chen et al., 2016). Both T80 and T60 have the same alkyl chain length. However, T80 has a double bond (C18:1), which will increase the randomness of the chain region making it more fluid-like. Consequently, this increases the hydrophilicity of the surface. Therefore, T80 is a better co-surfactant which improves the stability of many drug carrier formulations.

Table 4.5: Summary of literatures finding using Tween series as co-surfactants and results from the current work.

Ref	System	Co-surfactant	Some extracted results
Current work (Sazalee et al., 2017)	Hexosomes nanoparticles (Hnp) from anomeric mixture of branched-chain Guerbet glycolipid ($\alpha\beta$-Glu-OC$_{10}$C$_6$)	T20, T40, T60, T80	Stability order of Hnp with co-surfactant: T80 > T60 > T40 > T20. Hnp with T80 reduces in the CAC value, smaller hydrodynamic size and most stable dispersed more than 6 weeks.
(Soliman et al., 2017)	Avanafil nanoparticles (AVnp)	T80, polyvinyl alcohol (PVA), Pluronic F68	T80 is more effective stabiliser for AVnp compared with F68 and PVA. T80 stabilised formulas (1:2 or 1:4) have low zeta potential due to shielding effect.

Table 4.5, continued.

Ref	System	Co-surfactant	Some extracted results
			AVnp with T80 (*in vitro* study) has better oral bioavailability and stability due to high solubility.
(Shah et al., 2016)	Surface coating with PTFE-water interface	T20, T60, T80, Brij 010, Brij 35, Brij 98	Stability of PTFE with co-surfactants: T60 > T20 > T80. PTFE with T80 has poor stability sedimentation. The double bond in T80 produce a kink making surface coating of PTFE less homogeneous and less stable.
(Jiang et al., 2017)	Ultrafiltration membranes Poly (L-lactic acid) (PLLA)	T80	Addition of T80 in PLLA increases the permeability and molecular weight cut–off of the membrane; favours formation of large pore and improves the miscibility between solvent and coagulant.
(Chen et al., 2016)	Procyanidins ultradeformable liposomes (PUDLs)	Span 20, T80, sodium deoxycholate	PUDLs containing T80 has high entrapment efficiency, a small particle size, high elasticity and prolonged drug release.
(Zhao et al., 2010)	Gold nanoparticles (Gnp)	T20, T40, T60, T80	Stability order of Gnp with co-surfactants: T80 > T60 > T40 > T20. Gnp with T80 reduces aggregation problem during centrifugation and remain disperse in biological media.
(Barauskas et al., 2006)	Sponge nanoparticles (SPnp) from diglycerol monooleate (DGMO) and glycerol dioleate (DGO)	T80	SPnp with co-surfactant T80 has good stability and no change in mean particles size and distribution. Addition of T80 has the advantage in drug delivery application.

CHAPTER 5: CONCLUSION

In this study, nature-like branched-chain glycolipid anomeric mixture of 2-hexyldecyl-$\beta(/\alpha)$-D-glucoside ($\alpha\beta$-Glu-OC$_{10}$C$_6$) has been studied using DSC, OPM and SAXS. The $\alpha\beta$-Glu-OC$_{10}$C$_6$ showed a melting temperature about 54°C. In anhydrous condition, $\alpha\beta$-Glu-OC$_{10}$C$_6$ formed a hexagonal (or columnar) phase as characterised by a focal conic texture while, in contact penetration technique, $\alpha\beta$-Glu-OC$_{10}$C$_6$ shows the isotropic phase (L) to the inverse hexagonal phase (H_{II}). SAXS measurement confirmed the OPM results in which $\alpha\beta$-Glu-OC$_{10}$C$_6$ is mainly characterised by a hexagonal phase in dried and hydrated form at the room temperature.

When dispersed in water using the top-down approached at room temperature, the nonionic branched-chain glycolipid surfactant, $\alpha\beta$-Glu-OC$_{10}$C$_6$ formed an inverse hexagonal liquid crystalline dispersions called hexosomes. Upon the addition of Tween series (T20, T40, T60 and T80) to the branched-chain glycolipid and water, the resulting dispersions have critical aggregation concentrations (CACs) smaller than a similar dispersion without co-surfactant. Thus, the co-surfactant improves the stability of the dispersion. Among those co-surfactants, T80 produced the smallest CAC value and smallest particle size compared to other co-surfactants. Moreover, the addition of Tween series especially T80 to the $\alpha\beta$-Glu-OC$_{10}$C$_6$ dispersion induced the formation of inverse hexagonal phase with a higher stability. The formation of mixed surfactant hexosomes was further studies in terms of their particle size and morphology using a particle sizer and a transmission electron microscope (TEM), respectively. From the measurement of particle size, the addition of co-surfactant (Tween series) decreased the average hydrodynamic size and reduced the PDI of the mixtures at the ratio of 10:1 of $\alpha\beta$-Glu-OC$_{10}$C$_6$:Tween series hexosomes. The mixtures of $\alpha\beta$-Glu-OC$_{10}$C$_6$:Tween series hexosomes were visualised by TEM and indicated that hexagonal or spherically shaped

particles were formed with size ranging between 30 to 90 nm in diameter compared to $\alpha\beta$-Glu-OC$_{10}$C$_6$ hexosomes with particles size of about 50-120 nm.

The stability of particle size variation and particle migration of branched-chain glycolipids hexosomes and mixed branched-chain glycolipids co-surfactant Tween series hexosomes measured by light backscattering measurements. Compared to those co-surfactants, $\alpha\beta$-Glu-OC$_{10}$C$_6$:T80 hexosome shows a consistent particle size without any occurance of sedimentation occur for the peak thickness kinetics throughout 24 h. Moreover, the stability of the $\alpha\beta$-Glu-OC$_{10}$C$_6$ and mixture of 10:1 of $\alpha\beta$-Glu-OC$_{10}$C$_6$:Tween series hexosomes were also studied using particle sizer at 25°C and 40°C. The $\alpha\beta$-Glu-OC$_{10}$C$_6$:T80 hexosome was the most stable dispersion after 1 month and also the smallest average hydrodynamic size during storage at 40°C compared to the storage at 25°C. Therefore, $\alpha\beta$-Glu-OC$_{10}$C$_6$:T80 hexosome has a good long term stability, and thus T80 is the best co-surfactant which can improve the stability of many drug carrier systems.

For future work, the mixture of $\alpha\beta$-Glu-OC$_{10}$C$_6$:T80 hexosome dispersion will be further explored as a drug carrier with an environmental-friendly active ingredient for suitable pharmaceutical and cosmetic applications.

REFERENCES

Ahmad, N., Ramsch, R., Esquena, J., Solans, C., Tajuddin, H. A., & Hashim, R. (2012). Physicochemical characterization of natural-like branched-chain glycosides toward formation of hexosomes and vesicles. *Langmuir, 28*(5), 2395-2403.

Ali, F., Wang, J., & Ullah, N. (2019). Oil/fat blending strategy for improving milk fat globule membrane stability and its effect on fatty acid composition. *International Journal of Dairy Technology*. Doi:10.1111/1471-0307.12604

Allec, N., Choi, M., Yesupriya, N., Szychowski, B., White, M. R., Kann, M. G., . . . Badano, A. (2015). Small-angle X-ray scattering method to characterize molecular interactions: Proof of concept. *Scientific Reports, 5*, Article #12085.

Allen, H. J., & Kisailus, E. C. (1992). *Glycoconjugates:Composition, structure, and function.* New York, NY: CRC Press.

Amar-Yuli, I., Wachtel, E., Shoshan, E. B., Danino, D., Aserin, A., & Garti, N. (2007). Hexosome and hexagonal phases mediated by hydration and polymeric stabilizer. *Langmuir, 23*(7), 3637-3645.

Azema, N. (2006). Sedimentation behaviour study by three optical methods - granulometric and electrophoresis measurements, dispersion optical analyser. *Powder Technology, 165*(3), 133-139.

Barauskas, J., Misiunas, A., Gunnarsson, T., Tiberg, F., & Johnsson, M. (2006). "Sponge" nanoparticle dispersions in aqueous mixtures of diglycerol monooleate, glycerol dioleate, and polysorbate 80. *Langmuir, 22*(14), 6328-6334.

Barón, M. (2001). Definitions of basic terms relating to low-molar-mass and polymer liquid crystals (IUPAC Recommendations 2001). *Pure and Applied Chemistry, 73*(5), 845-895.

Berne, B. J., & Pecora, R. (2000). *Dynamic light scattering: with applications to chemistry, biology, and physics.* New York, NY: Courier Corporation.

Bhattacharya, M., & Dixit, S. G. (2015). Study of mixed micelles of sodium dodecyl sulphate and nonionic surfactants polysorbates tween series: Their interaction and thermodynamic parameter using cyclic voltammetry. *International Journal of Chemical Studies, 3*(3), 22-25.

Blunk, D., Bongartz, N., Stubenrauch, C., & Gärtner, V. (2009). Syntheses, amphitropic liquid crystallinity, and surface activity of new inositol-based amphiphiles. *Langmuir, 25*(14), 7872-7878.

Boyd, B., Davey, G., Khoo, S., & Whittaker, D. (2005). Compositions and methods of delivery of biologically active agents. *International Patent WO2005021046*.

Boyd, B. J., Rizwan, S. B., Dong, Y.-D., Hook, S., & Rades, T. (2007). Self-assembled geometric liquid-crystalline nanoparticles imaged in three dimensions: hexosomes are not necessarily flat hexagonal prisms. *Langmuir, 23*(25), 12461-12464.

Boyd, J. V., Parkinson, C., & Sherman, P. (1972). Factors affecting emulsion stability, and the HLB concept. *Journal of Colloid and Interface Science, 41*(2), 359-370.

Brooks, N. J., Hamid, H. A., Hashim, R., Heidelberg, T., Seddon, J. M., Conn, C. E., . . . Hussen, R. S. D. (2011). Thermotropic and lyotropic liquid crystalline phases of Guerbet branched-chain-D-glucosides. *Liquid Crystals, 38*(11-12), 1725-1734.

Burchard, W. (1983). Static and dynamic light scattering from branched polymers and biopolymers. *Light Scattering from Polymers* (pp. 1-124). Switzerland: Springer.

Buron, H., Mengual, O., Meunier, G., Cayré, I., & Snabre, P. (2004). Optical characterization of concentrated dispersions: applications to laboratory analyses and on-line process monitoring and control. *Polymer International, 53*(9), 1205-1209.

Castaldo, S., & Capasso, F. (2002). Propolis, an old remedy used in modern medicine. *Fitoterapia, 73*, S1-S6.

Celia, C., Trapasso, E., Cosco, D., Paolino, D., & Fresta, M. (2009). Turbiscan Lab expert analysis of the stability of ethosomes and ultradeformable liposomes containing a bilayer fluidizing agent. *Colloids and Surfaces B: Biointerfaces, 72*(1), 155-160.

Chai, Z., Zeng, M., Ren, Y., Zhang, R., Feng, L., & Zhao, Z. (2019). A prediction method on the static stability of coal water mixture. *Energy & Fuels*. Doi:10.1021/acs.energyfuels.9b00082

Chen, R., Li, R., Liu, Q., Bai, C., Qin, B., Ma, Y., & Han, J. (2016). Ultradeformable liposomes: a novel vesicular carrier for enhanced transdermal delivery of procyanidins: Effect of surfactants on the formation, stability, and transdermal

delivery. *An Official Journal of the American Association of Pharmaceutical Scientists*, 1-10.

Chen, Y., Liang, X., Ma, P., Tao, Y., Wu, X., Wu, X., . . . Gui, S. (2015). Phytantriol-based in situ liquid crystals with long-term release for intra-articular administration. *An Official Journal of the American Association of Pharmaceutical Scientists, 16*(4), 846-854.

Chen, Y., Ma, P., & Gui, S. (2014). Cubic and hexagonal liquid crystals as drug delivery systems. *BioMed Research International, 2014,* 1-12.

Cohen-Avrahami, M., Aserin, A., & Garti, N. (2010). H_{II} mesophase and peptide cell-penetrating enhancers for improved transdermal delivery of sodium diclofenac. *Colloids and Surfaces B: Biointerfaces, 77*(2), 131-138.

Cohen-Avrahami, M., Libster, D., Aserin, A., & Garti, N. (2012). Penetratin-induced transdermal delivery from H_{II} mesophases of sodium diclofenac. *Journal of Controlled Release, 159*(3), 419-428.

Collings, P. J., & Hird, M. (1997). *Introduction to liquid crystals: Chemistry and physics*. London, England: Talyor & Francis.

Craievich, A. F. (2018). Small-angle X-ray scattering by nanostructured materials. *Handbook of Sol-Gel Science and Technology: Processing, Characterization and Applications*, 1185-1230.

Crommelin, D. J., Storm, G., & Luijten, P. (2011). 'Personalised medicine' through 'personalised medicines': time to integrate advanced, non-invasive imaging approaches and smart drug delivery systems. *International Journal of Pharmaceutics, 415*(1-2), 5-8.

Curatolo, W. (1987). Glycolipid function. *Biochimica et Biophysica Acta (BBA)-Reviews on Biomembranes, 906*(2), 137-160.

Diamant, H., & Andelman, D. (1999). Onset of self-assembly in polymer-surfactant systems. *A Letters Journal Exploring The Frontiers of Physics, 48*(2), 170-176

Dierking, I. (2003). *Textures of liquid crystals*. Federal Republic of Germany: John Wiley & Sons.

Domingos, R. F., Baalousha, M. A., Ju-Nam, Y., Reid, M. M., Tufenkji, N., Lead, J. R., . . . Wilkinson, K. J. (2009). Characterizing manufactured nanoparticles in the environment: multimethod determination of particle sizes. *Environmental Science & Technology, 43*(19), 7277-7284.

Dong, Y.-D., Larson, I., Barnes, T. J., Prestidge, C. A., & Boyd, B. J. (2011). Adsorption of nonlamellar nanostructured liquid-crystalline particles to biorelevant surfaces for improved delivery of bioactive compounds. *ACS Applied Materials & Interfaces, 3*(5), 1771-1780.

Farn, R. J. (2008). *Chemistry and technology of surfactants*. Federal Republic of Germany: John Wiley & Sons.

Filella, M., Zhang, J., Newman, M. E., & Buffle, J. (1997). Analytical applications of photon correlation spectroscopy for size distribution measurements of natural colloidal suspensions: capabilities and limitations. *Colloids and Surfaces A: Physicochemical and Engineering Aspects, 120*(1), 27-46.

Fissan, H., Ristig, S., Kaminski, H., Asbach, C., & Epple, M. (2014). Comparison of different characterization methods for nanoparticle dispersions before and after aerosolization. *Analytical Methods, 6*(18), 7324-7334.

Fong, W.-K., Hanley, T., & Boyd, B. J. (2009). Stimuli responsive liquid crystals provide 'on-demand' drug delivery *in vitro* and *in vivo*. *Journal of Controlled Release, 135*(3), 218-226.

Gabr, M. M., Mortada, S. M., & Sallam, M. A. (2017). Hexagonal liquid crystalline nanodispersions proven superiority for enhanced oral delivery of rosuvastatin: *in vitro* characterization and *in vivo* pharmacokinetic study. *Journal of Pharmaceutical Sciences, 106*(10), 3103-3112.

Galliková, D., Liskayová, G., Búcsi, A., Hubčík, L., Martínez, J., & Uhríková, D. (2018). DOPE-oleic acid-Ca2$^+$ as DNA condensing agent. *European Pharmaceutical Journal, 65*(1), 1-9.

Garofalakis, G., Murray, B. S., & Sarney, D. B. (2000). Surface activity and critical aggregation concentration of pure sugar esters with different sugar headgroups. *Journal of Colloid and Interface Science, 229*(2), 391-398.

González-Reza, R., Quintanar-Guerrero, D., Del Real-Lopez, A., Pinon-Segundo, E., & Zambrano-Zaragoza, M. (2018). Effect of sucrose concentration and pH onto the physical stability of β-carotene nanocapsules. *Food Science and Technology, 90*, 354-361.

Goodby, J. (1998). Liquid crystals and life. *Liquid Crystals, 24*(1), 25-38.

Goodby, J., Görtz, V., Cowling, S., Mackenzie, G., Martin, P., Plusquellec, D., . . . Queneau, Y. (2007). Thermotropic liquid crystalline glycolipids. *Chemical Society Reviews, 36*(12), 1971-2032.

Goodby, J. W. (2014). Introduction to defect textures in liquid crystals. *Handbook of Visual Display Technology*, 1-23.

Guo, C., Wang, J., Cao, F., Lee, R. J., & Zhai, G. (2010). Lyotropic liquid crystal systems in drug delivery. *Drug Discovery Today, 15*(23), 1032-1040.

Guo, Z., Zhang, Y., DuanMu, Y., Xu, L., Xie, S., & Gu, N. (2006). Facile synthesis of micrometer-sized gold nanoplates through an aniline-assisted route in ethylene glycol solution. *Colloids and Surfaces A: Physicochemical and Engineering Aspects, 278*(1-3), 33-38.

Guo, Z., Zhang, Y., Mao, Y., Huang, L., & Gu, N. (2006). Synthesis of microsized gold nanoplates by a self-seeding method in ethanol solution. *Materials Letters, 60*(29-30), 3522-3525.

Gustafsson, J., Ljusberg-Wahren, H., Almgren, M., & Larsson, K. (1997). Submicron particles of reversed lipid phases in water stabilized by a nonionic amphiphilic polymer. *Langmuir, 13*(26), 6964-6971.

Hashim, R., Hashim, H. H. A., Rodzi, N. Z. M., Hussen, R. S. D., & Heidelberg, T. (2006). Branched chain glycosides: Enhanced diversity for phase behavior of easily accessible synthetic glycolipids. *Thin Solid Films, 509*(1), 27-35.

Hashim, R., Mirzadeh, S. M., Heidelberg, T., Minamikawa, H., Yoshiaki, T., & Sugimura, A. (2011). A reevaluation of the epimeric and anomeric relationship of glucosides and galactosides in thermotropic liquid crystal self-assemblies. *Carbohydrate Research, 346*(18), 2948-2956.

Hashim, R., Sugimura, A., Minamikawa, H., & Heidelberg, T. (2012). Nature-like synthetic alkyl branched-chain glycolipids: a review on chemical structure and self-assembly properties. *Liquid Crystals, 39*(1), 1-17.

Hashim, R., Zahid, N. I., Aripin, N. F. K., Ogawa, S., & Sugimura, A. (2018). Dry thermotropic glycolipid self-assembly: A review. *Journal of Oleo Science, 67*(6), 651-668.

Hato, M. (2001). Synthetic glycolipid/water systems. *Current Opinion in Colloid & Interface Science, 6*(3), 268-276.

Hato, M., Minamikawa, H., Salkar, R. A., & Matsutani, S. (2002). Alkylglycosides with an isoprenoid-type hydrophobic chain can afford greater control of aqueous phase structures at low temperatures. *Langmuir, 18*(9), 3425-3429.

Hirlekar, R., Jain, S., Patel, M., Garse, H., & Kadam, V. (2010). Hexosomes: A novel drug delivery system. *Current Drug Delivery, 7*(1), 28-35.

Holmberg, K. (2001). Natural surfactants. *Current Opinion in Colloid & Interface Science, 6*(2), 148-159.

Huibers, P. D., & Shah, D. O. (1997). Evidence for synergism in nonionic surfactant mixtures: enhancement of solubilization in water-in-oil microemulsions. *Langmuir, 13*(21), 5762-5765.

Hyde, S. T. (2001). Identification of lyotropic liquid crystalline mesophases. *Handbook of Applied Surface and Colloid Chemistry,* 299-323.

Israelachvili, J. N. (1994). The science and applications of emulsions—an overview. *Colloids and Surfaces A: Physicochemical and Engineering Aspects, 91*, 1-8.

Israelachvili, J. N. (2011). *Intermolecular and surface forces*. USA: Academic press.

Israelachvili, J. N., Marčelja, S., & Horn, R. G. (1980). Physical principles of membrane organization. *Quarterly Reviews of Biophysics, 13*(2), 121-200.

Israelachvili, J. N., Mitchell, D. J., & Ninham, B. W. (1976). Theory of self-assembly of hydrocarbon amphiphiles into micelles and bilayers. *Journal of the Chemical Society, Faraday Transactions 2: Molecular and Chemical Physics, 72*, 1525-1568.

Jiang, B., Wang, B., Zhang, L., Sun, Y., Xiao, X., Yang, N., & Dou, H. (2017). Effect of Tween 80 on morphology and performance of poly (L-lactic acid) ultrafiltration membranes. *Journal of Applied Polymer Science, 134*(5), 1-9.

Kitamoto, D., Isoda, H., & Nakahara, T. (2002). Functions and potential applications of glycolipid biosurfactants from energy-saving materials to gene delivery carriers. *Journal of Bioscience and Bioengineering, 94*(3), 187-201.

Kitamoto, D., Morita, T., Fukuoka, T., Konishi, M.-a., & Imura, T. (2009). Self-assembling properties of glycolipid biosurfactants and their potential applications. *Current Opinion in Colloid & Interface Science, 14*(5), 315-328.

Kothekar, S. C., Ware, A. M., Waghmare, J. T., & Momin, S. (2007). Comparative analysis of the properties of Tween-20, Tween-60, Tween-80, Arlacel-60, and Arlacel-80. *Journal of Dispersion Science and Technology, 28*(3), 477-484.

Koltover, I., Salditt, T., Rädler, J. O., & Safinya, C. R. (1998). An inverted hexagonal phase of cationic liposome-DNA complexes related to DNA release and delivery. *Science, 281*(5373), 78-81.

Kronberg, B., & Lindman, B. (2003). *Surfactants and polymers in aqueous solution*: John Wiley & Sons Ltd., Chichester.

Kulkarni, C. (2016). Lipid self-assemblies and nanostructured emulsions for cosmetic formulations. *Cosmetics, 3*(4), 1-15.

Kumar, G. P., & Rajeshwarrao, P. (2011). Nonionic surfactant vesicular systems for effective drug delivery - an overview. *Acta Pharmaceutica Sinica B, 1*(4), 208-219.

Laughlin, R. G. (1992). The role of swelling methods in surfactant phase science: past, present, and future. *Advances in Colloid and Interface Science, 41*, 57-79.

Laurent, N., Lafont, D., Dumoulin, F., Boullanger, P., Mackenzie, G., Kouwer, P. H., & Goodby, J. W. (2003). Synthesis of amphiphilic phenylazophenyl glycosides and a study of their liquid crystal properties. *Journal of the American Chemical Society, 125*(50), 15499-15506.

Lee, K. W., Nguyen, T.-H., Hanley, T., & Boyd, B. J. (2009). Nanostructure of liquid crystalline matrix determines in vitro sustained release and in vivo oral absorption kinetics for hydrophilic model drugs. *International Journal of Pharmaceutics, 365*(1-2), 190-199.

Lemarchand, C., Couvreur, P., Besnard, M., Costantini, D., & Gref, R. (2003). Novel polyester-polysaccharide nanoparticles. *Pharmaceutical Research, 20*(8), 1284-1292.

Lemarchand, C., Couvreur, P., Vauthier, C., Costantini, D., & Gref, R. (2003). Study of emulsion stabilization by graft copolymers using the optical analyzer Turbiscan. *International Journal of Pharmaceutics, 254*(1), 77-82.

Liew, C. Y., Salim, M., Zahid, N. I., & Hashim, R. (2015). Biomass derived xylose Guerbet surfactants: thermotropic and lyotropic properties from small-angle X-ray scattering. *RSC Advances, 5*(120), 99125-99132.

Loewenstein, A., & Igner, D. (1991). Deuterium NMR studies of n-octyl *α* and *β*-glucopyranoside liquid-crystalline systems. *Liquid Crystals, 10*(4), 457-466.

Loi, C. C., Eyres, G. T., & Birch, E. J. (2019). Effect of mono-and diglycerides on physical properties and stability of a protein-stabilised oil-in-water emulsion. *Journal of Food Engineering, 240*, 56-64.

Londoño, O. M., Tancredi, P., Rivas, P., Muraca, D., Socolovsky, L. M., & Knobel, M. (2018). Small-angle X-ray scattering to analyze the morphological properties of nanoparticulated systems. *Handbook of materials characterization* (pp. 37-75) Switzerland: Springer Nature.

Lopes, L. B., Ferreira, D. A., de Paula, D., Garcia, M. T. J., Thomazini, J. A., Fantini, M. C., & Bentley, M. V. L. (2006). Reverse hexagonal phase nanodispersion of monoolein and oleic acid for topical delivery of peptides: in vitro and in vivo skin penetration of cyclosporin A. *Pharmaceutical Research, 23*(6), 1332-1342.

Lopes, L. B., Lopes, J. L., Oliveira, D. C., Thomazini, J. A., Garcia, M. T. J., Fantini, M. C., . . . Bentley, M. V. L. (2006). Liquid crystalline phases of monoolein and water for topical delivery of cyclosporin A: characterization and study of in vitro and in vivo delivery. *European Journal of Pharmaceutics and Biopharmaceutics, 63*(2), 146-155.

Lopes, L. B., Speretta, F. F., & Bentley, M. V. L. (2007). Enhancement of skin penetration of vitamin K using monoolein-based liquid crystalline systems. *European Journal of Pharmaceutical Sciences, 32*(3), 209-215.

Lu, T., & Guo, H. (2018). Phase behavior of lipid bilayers: A dissipative particle dynamics simulation study. *Advanced Theory and Simulations, 1*(5), 1-13.

Mannock, D. A., Akiyama, M., Lewis, R. N., & McElhaney, R. N. (2000). Synthesis and thermotropic characterization of a homologous series of racemic β-d-glucosyl dialkylglycerols. *Biochimica et Biophysica Acta (BBA)-Biomembranes, 1509*(1), 203-215.

Menczel, J. D., Judovits, L., Prime, R. B., Bair, H. E., Reading, M., & Swier, S. (2009). Differential scanning calorimetry (DSC). In J.D. Menczel & R.B. Prime (Eds.), *Thermal Analysis of Polymers: Fundamentals and Applications* (pp.7-239). England: John Wiley & Sons.

Mengual, O., Meunier, G., Cayre, I., Puech, K., & Snabre, P. (1999). Characterisation of instability of concentrated dispersions by a new optical analyser: The TURBISCAN MA 1000. *Colloids and Surfaces A: Physicochemical and Engineering Aspects, 152*(1), 111-123.

Mengual, O., Meunier, G., Cayré, I., Puech, K., & Snabre, P. (1999). TURBISCAN MA 2000: multiple light scattering measurement for concentrated emulsion and suspension instability analysis. *Talanta, 50*(2), 445-456.

Murthy, S. K. (2007). Nanoparticles in modern medicine: state of the art and future challenges. *International Journal of Nanomedicine, 2*(2), 129-141.

Nagarajan, R. (2002). Molecular packing parameter and surfactant self-assembly: The neglected role of the surfactant tail. *Langmuir, 18*(1), 31-38.

Neto, C., Aloisi, G., Baglioni, P., & Larsson, K. (1999). Imaging soft matter with the atomic force microscope: Cubosomes and hexosomes. *The Journal of Physical Chemistry B, 103*(19), 3896-3899.

Nguan, H., Heidelberg, T., Hashim, R., & Tiddy, G. (2010). Quantitative analysis of the packing of alkyl glycosides: A comparison of linear and branched alkyl chains. *Liquid Crystals, 37*(9), 1205-1213.

Nguyen, T. H., Hanley, T., Porter, C. J., & Boyd, B. J. (2011). Nanostructured liquid crystalline particles provide long duration sustained-release effect for a poorly water soluble drug after oral administration. *Journal of Controlled Release, 153*(2), 180-186.

Nielsen, S. O., Lopez, C. F., Ivanov, I., Moore, P. B., Shelley, J. C., & Klein, M. L. (2004). Transmembrane peptide-induced lipid sorting and mechanism of L_α-to-inverted phase transition using coarse-grain molecular dynamics. *Biophysical Journal, 87*(4), 2107-2115.

O'neill, M. (1966). Measurement of specific heat functions by differential scanning calorimetry. *Analytical Chemistry, 38*(10), 1331-1336.

Pabst, G., Kučerka, N., Nieh, M.-P., Rheinstädter, M., & Katsaras, J. (2010). Applications of neutron and X-ray scattering to the study of biologically relevant model membranes. *Chemistry and Physics of Lipids, 163*(6), 460-479.

Pecora, R. (2013). *Dynamic light scattering: Applications of photon correlation spectroscopy*. California: Springer Science & Business Media.

Perutková, Š., Daniel, M., Dolinar, G., Rappolt, M., Kralj‑Iglič, V., & Iglič, A. (2009). Stability of the inverted hexagonal phase. *Advances in Planar Lipid Bilayers and Liposomes, 9*, 237-278.

Perutková, Š., Daniel, M., Rappolt, M., Pabst, G., Dolinar, G., Kralj-Iglič, V., & Iglič, A. (2011). Elastic deformations in hexagonal phases studied by small-angle X-ray diffraction and simulations. *Physical Chemistry Chemical Physics, 13*(8), 3100-3107.

Posocco, P., Perazzo, A., Preziosi, V., Laurini, E., Pricl, S., & Guido, S. (2016). Interfacial tension of oil/water emulsions with mixed non-ionic surfactants: comparison between experiments and molecular simulations. *RSC Advances, 6*(6), 4723-4729.

Pouzot, M., Mezzenga, R., Leser, M., Sagalowicz, L., Guillot, S., & Glatter, O. (2007). Structural and rheological investigation of *Fd3m* inverse micellar cubic phases. *Langmuir, 23*(19), 9618-9628.

Rappolt, M. (2006). The biologically relevant lipid mesophases as "seen" by X-rays. *Advances in Planar Lipid Bilayers and Liposomes, 5*, 253-283.

Rappolt, M., Hickel, A., Bringezu, F., & Lohner, K. (2003). Mechanism of the lamellar/inverse hexagonal phase transition examined by high resolution X-ray diffraction. *Biophysical Journal, 84*(5), 3111-3122.

Rendall, K., Tiddy, G. J., & Trevethan, M. A. (1983). Optical microscopy and nuclear magnetic resonance studies of mesophases formed at compositions between hexagonal and lamellar phases in sodium n-alkanoate+ water mixtures and related surfactant systems. *Journal of the Chemical Society, Faraday Transactions 1: Physical Chemistry in Condensed Phases, 79*(3), 637-649.

Revathi, S., & Dhanaraju, M. (2014). Hexosomes as a novel drug delivery system: A review. *Internal Journal of Pharmaceutical Sciences and Research, 6*, 58-63.

Ribeiro, I. R., Immich, M. F., Lundberg, D., Poletto, F., & Loh, W. (2019). Physiological neutral pH drives a gradual lamellar-to-reverse cubic-to-reverse hexagonal phase transition in phytantriol-based nanoparticles. *Colloids and Surfaces B: Biointerfaces, 177*, 204-210.

Robinson, P. C., & Davidson, M. W. (2016). Polarized light microscopy. Retrieved on October 3, 2016 from https://www.microscopyu.com/techniques/polarized-light/polarized-light-microscopy

Rosen, M. J., & Kunjappu, J. T. (2004). *Surfactants and Interfacial Phenomena* (Vol. 82) New Jersey: Wiley Online Library.

Ryu, V., McClements, D. J., Corradini, M. G., & McLandsborough, L. (2018). Effect of ripening inhibitor type on formation, stability, and antimicrobial activity of thyme oil nanoemulsion. *Food Chemistry, 245*, 104-111.

Sagalowicz, L., Mezzenga, R., & Leser, M. E. (2006). Investigating reversed liquid crystalline mesophases. *Current Opinion in Colloid & Interface Science, 11*(4), 224-229.

Sagar, G. H., Arunagirinathan, M., & Bellare, J. R. (2007). Self-assembled surfactant nano-structures important in drug delivery: A review. *Indian Journal of Experimental Biology, 45*(2), 133-159.

Sagnella, S. M., Conn, C. E., Krodkiewska, I., & Drummond, C. J. (2009). Soft ordered mesoporous materials from nonionic isoprenoid-type monoethanolamide amphiphiles self-assembled in water. *Soft Matter, 5*(23), 4823-4834.

Salager, J.-L. (2002). Surfactants types and uses. *FIRP Booklet # E300-A*, 1-40.

Salim, M., Zahid, N. I., Liew, C. Y., & Hashim, R. (2015). Cubosome particles of a novel Guerbet branched chain glycolipid. *Liquid Crystals, 43*(2), 168-174.

Sandoval-Altamirano, C., Sanchez, S., Pizarro, N., Morales, J., & Gunther, G. (2019). Alkyl-mannoside derivatives: Glycolipids able to form big size aggregates. *Journal of Physical Organic Chemistry, 32*(1), Article #3822.

Sani, F. A., Heidelberg, T., & Hashim, R. (2012). Alkyl triazole glycosides (ATGs) - A new class of bio-related surfactants. *Colloids and Surfaces B: Biointerfaces, 97*, 196-200.

Sazalee, S. A., Ahmad, N., & Hashim, R. (2017). Investigation of self-assembly properties and the effect of Tween series co-surfactants on the stability of nonionic branched-chain glycolipid hexosomes. *Colloids and Surfaces A: Physicochemical and Engineering Aspects, 529*, 210-221.

Seddon, J., Robins, J., Gulik-Krzywicki, T., & Delacroix, H. (2000). Inverse micellar phases of phospholipids and glycolipids. Invited Lecture. *Physical Chemistry Chemical Physics, 2*(20), 4485-4493.

Seddon, J. M. (1990). Structure of the inverted hexagonal (H_{II}) phase, and non-lamellar phase transitions of lipids. *Biochimica et Biophysica Acta (BBA)-Reviews on Biomembranes, 1031*(1), 1-69.

Seddon, J. M., Squires, A. M., Conn, C. E., Ces, O., Heron, A. J., Mulet, X., . . . Templer, R. H. (2006). Pressure-jump X-ray studies of liquid crystal transitions in lipids. *Philosophical Transactions of the Royal Society A: Mathematical, Physical and Engineering Sciences, 364*(1847), 2635-2655.

Sekhar, K. P., Bangal, P. R., & Nayak, R. R. (2019). A systematic surface studies on the glycolipids to understand the surface adsorption behavior. *Colloids and Surfaces A: Physicochemical and Engineering Aspects, 563*, 226-236.

Shah, V., Bharatiya, B., Shukla, A. D., Mukherjee, T., & Shah, D. O. (2016). Adsorption of nonionic Brij and Tween surfactants at PTFE-water and air-water interfaces: Investigations on wetting, dispersion stability, foaming and drug solubilization. *Colloids and Surfaces A: Physicochemical and Engineering Aspects, 508*, 159-166.

Sharma, S. C., Kunieda, H., Esquena, J., & Abreu, C. R. (2006). Phase behavior and preparation of mesoporous silica in aqueous mixtures of fluorinated surfactant and hydrophobic fluorinated polymer. *Journal of Colloid and Interface Science, 299*(1), 297-304.

Shearman, G., Ces, O., Templer, R., & Seddon, J. (2006). Inverse lyotropic phases of lipids and membrane curvature. *Journal of Physics: Condensed Matter, 18*(28), S1105-S1124.

Shibaev, V., & Danilov, L. (1992). New developments in the synthesis of phosphopolyprenols and their glycosyl esters. *Biochemistry and Cell Biology, 70*(6), 429-437.

Siegel, D. (1986). Inverted micellar intermediates and the transitions between lamellar, cubic, and inverted hexagonal lipid phases: Mechanism of the L_{α}-H_{II} phase transitions. *Biophysical Journal, 49*(6), 1155-1170.

Soliman, K. A., Ibrahim, H. K., & Ghorab, M. M. (2017). Effects of different combinations of nanocrystallization technologies on avanafil nanoparticles: *in vitro*, *in vivo* and stability evaluation. *International Journal of Pharmaceutics, 517*(1), 148-156.

Sum, C. H., Wettig, S., & Slavcev, R. A. (2014). Impact of DNA vector topology on non-viral gene therapeutic safety and efficacy. *Current Gene Therapy, 14*(4), 309-329.

Sun, R. G., & Zhang, J. (2004). The cubic phase of phosphatidylethanolamine film by small angle x-ray scattering. *Journal of Physics D: Applied Physics, 37*(3), 463-467.

Svergun, D. I., Koch, M. H., Timmins, P. A., & May, R. P. (2013). *Small Angle X-ray and Neutron Scattering from Solutions of Biological Macromolecules* (Vol. 19). New York, NY: Oxford University Press.

Swarnakar, N. K., Jain, V., Dubey, V., Mishra, D., & Jain, N. (2007). Enhanced oromucosal delivery of progesterone via hexosomes. *Pharmaceutical Research, 24*(12), 2223-2230.

Tan, K. H., Tajuddin, H. A., & Johan, M. R. (2015). Feasibility study on the use of the seeding growth technique in producing a highly stable gold nanoparticle colloidal system. *Journal of Nanomaterials, 2015*, 1-8.

Tanford, C. (1972). Micelle shape and size. *The Journal of Physical Chemistry, 76*(21), 3020-3024.

Tate, M. W., & Gruner, S. M. (1989). Temperature dependence of the structural dimensions of the inverted hexagonal (H_{II}) phase of phosphatidylethanolamine-containing membranes. *Biochemistry, 28*(10), 4245-4253.

Taylor, D., Thomas, R., & Penfold, J. (2007). Polymer/surfactant interactions at the air/water interface. *Advances in Colloid and Interface Science, 132*(2), 69-110.

Thadanki, M., Srivalli, P., & Prabha, K. (2011). Overview of cubosomes: A nanoparticle. *International Journal of Research in Pharmacy and Chemistry, 1*(3), 535-541.

Tschierske, C. (2007). Liquid crystal engineering - new complex mesophase structures and their relations to polymer morphologies, nanoscale patterning and crystal engineering. *Chemical Society Reviews, 36*(12), 1930-1970.

Tyler, A. I., Law, R. V., & Seddon, J. M. (2015). X-ray diffraction of lipid model membranes. *Methods in Membrane Lipids*, *1232*, 199-225.

Van Gestel, B. (2007). Differential Scanning Calorimetry. 5-39.

Vill, V., & Hashim, R. (2002). Carbohydrate liquid crystals: Structure–property relationship of thermotropic and lyotropic glycolipids. *Current Opinion in Colloid & Interface Science, 7*(5), 395-409.

Yaghmur, A., & Rappolt, M. (2013). The micellar cubic *Fd*3*m* phase: Recent advances in the structural characterization and potential applications. *Advances in Planar Lipid Bilayers and Liposomes, 18*, 111-145.

Yin, T., Yang, Z., Lin, M., Zhang, J., & Dong, Z. (2019). Aggregation kinetics and colloidal stability of amphiphilic janus nanosheets in aqueous solution. *Industrial & Engineering Chemistry Research, 58*(11), 4479-4486.

Zahid, N., Hashim, R., & Heidelberg, T. (2012). *Phase behaviour of nature-like branched-chain glycosides*. Paper presented at the UMT 11th International Annual Symposium on Sustainability Science and Management, Terengganu, Malaysia.

Zahid, N. I., Conn, C. E., Brooks, N. J., Ahmad, N., Seddon, J. M., & Hashim, R. (2013). Investigation of the effect of sugar stereochemistry on biologically relevant lyotropic phases from branched-chain synthetic glycolipids by small-angle X-ray scattering. *Langmuir, 29*(51), 15794-15804.

Zhao, Y., Wang, Z., Zhang, W., & Jiang, X. (2010). Adsorbed Tween 80 is unique in its ability to improve the stability of gold nanoparticles in solutions of biomolecules. *Nanoscale, 2*(10), 2114-2119.

Zied, O. K. A., Hashim, R., & Timimi, B. (2015). Amphitropic liquid crystal phases from polyhydroxy sugar surfactants: Fundamental studies. *Colloidal Nanoparticles for Biomedical Applications, 9338*, 18-28.

LIST OF PUBLICATION AND PAPER PRESENTED

Publication

Academic Journal

Sazalee, S. A., Ahmad, N., & Hashim, R. (2017). Investigation of self-assembly properties and the effect of Tween series co-surfactants on the stability of nonionic branched-chain glycolipid hexosomes. *Colloids and Surfaces A: Physicochemical and Engineering Aspects, 529*, 210-221.

Presentation

Poster

1. Self-Assembly Properties of Nonionic Branched-Chain Glycolipid: Effect of Co-Surfactant, 7th Asian Conference on Colloid and Interface Science (ACCIS 2017), 8th-10th August 2017, Berjaya Times Square, Kuala Lumpur, Malaysia (Presenter).

2. Self-Assembly Properties of Nonionic Branched-Chain Glycolipids: Effect of Co-Surfactant, Research Innovation & Design Exhibition (RIDE 2017), 26th July 2017, UiTM-MTDC Technopreneur Centre, Universiti Teknologi MARA (UiTM), Malaysia (Gold Medal).

3. Physico-chemical Characterization and Liquid Crystalline Properties of Branched-Chain Glucoside, 6th Asian Conference on Colloid and Interface Science (ACCIS 2015), 24th- 27th November 2015, Arkas Sasebo, Nagasaki, Japan (Presenter).